Structural Engineering of Safe Lithium-ion Batteries

Emmanuel Chisom Nwaogu (Masters Student**)**

Submitted in fulfillment of the requirements for the degree of Master of Science in Chemical and Materials Engineering.

NAZARBAYEV UNIVERSITY

School of Engineering and Digital Science
Department of Chemical and Materials Engineering
Nazarbayev University

53 Kabanbay Batyr Avenue,
Astana, Kazakhstan, 010000

Supervisor: Prof. Zhumabay Bakenov

Co-supervisor Dr. Arailym Nurpeissova

April, 2023

Declaration

I hereby, declare that this manuscript, entitled “Structural Engineering for Safe Lithium-ion Batteries”, Is the result of my own work except for quotations and citations which have been duly acknowledged.

I also declare that, to the best of my knowledge and belief, it has not been previously or concurrently submitted, in whole or in part, for any other degree or diploma at Nazarbayev University or any other national or international institution.

Emmanuel Chisom Nwaogu
Date: April 17, 2023

Abstract

To consider lithium-metal batteries a good choice for next-generation energy storage system, it is important to maintain a long-term cyclability and reduce the excess lithium metal deposits. The application of Li-metal batteries has been limited due to problem of dendrite formation caused by Li metal, including low Coulombic efficiency and short circuits. This study has focused on creating a three-dimensional (3D) copper current collector chosen to serve as anode materials by modifying it with 50 nm thickness of gold to promote deposition of Li metal without the formation of dendrites. The 3D-Cu current collector maintained lithiophilic properties after modification, which not only lowered the local current density but also provided a large surface area for Li deposition. After half-cell construction of Au-2D-Cu and Au-3D-Cu with Li-metal 0 mV overpotential was achieved after plating and stripping for above 24 hours. Furthermore, the Au-3D-Cu current collector showed superior properties when compared to 2D-Cu, 3D-Cu, and Au-2D-Cu in terms of longer stable cyclability and CE.

NCM cathode and 2D-Cu, 3D-Cu, Au-2D-Cu, and Au-3D-Cu current collectors were constructed separately as full cells, Au-3D||NCM full cell showed a high capacity of about 181 mAh g^{-1} at the first cycle and later decreased to 100 mAh g^{-1} after 100 cycles which is superior compared to the Au-2D||NMC, 2D||NCM, and 3D||NCM, which had 170 mAh g^{-1}, 164 mAh g^{-1}, and 160 mAh g^{-1} at first reversible capacity, and steadily decreased to 80, 20, and 15 after 100 cycles, respectively. Additionally, the use of high concentration tri-lithium salt electrolyte of 1.5M LiTFSI + 1M LiDFOB, + 0.05M LiPF6 in FEC/DDME (2:3 v/v) at 0.2 C contributed to achieving high capacity, capacity loss reduced, stable reversibility over a prolonged cycling, and high CE of 99.9% especially in the case of Au@3D||NCM also, the post mortem analysis with SEM confirmed the dendrite growth suppression in Au@3D||NCM after 100 cycles.

However, complex battery construction and capacity loss was the two major challenges the research faced due to limited supply of lithium. Fortunately, we were able to mitigate this problems by utilizing a high concentration tri-lithium salt electrolyte and modification of the current collector. For better result, I will recommend that more experiments should be conducted, varying different thickness of the sputtered gold ranging from 40 nm, 30 nm, and 25 nm. This approach may lead to more better and viable result in the future.

Acknowledgement

To begin with, I would like to sincerely appreciate my lead and Co-Supervisor, Professor Zhumabay Bakenov and Dr. Arailym Nurpeissova who have immensely supported me and my in all ramification, their daily weekly meeting, mentorship, advice and providing me with all the necessary materials and guidelines has helped to give me a positive finishing in my project. I would also like to state that they have always made themselves available regardless of their daily tight schedules in dishing out instruction and recommendations.

Secondly, I would also appreciate the advanced materials energy and application lab (Battery group) for their support so far in exchanging knowledge with me which has also supported my progress so far.

My appreciation will not be complete if I forget to say thank you to Nazarbayev University and the management for allowing me to enjoy this quality research experience which is highly competitive when compared with what is obtainable internationally.

Lastly, I would love to say thank you to my family and friends (Theresa Ike Amarachi). Who also calls and checks on me especially for my mental health. Thank you everyone.

Table of Contents

List of Abbreviations and Symbols

2D-CU	Two Dimensional Copper
3D-CU	Three Dimensional Copper
AFM	Atomic Force Microscopy
Al	Aluminum
AU	Gold
CC	Current Collector
Cu	Copper
CV	Cyclic Voltammetry
DEC	Diethyl Carbonate
DMC	Dimethyl carbonate
DME	Dimethoxymethane
EC	Ethylene carbonate
EDS	Energy-Dispersive X-ray spectroscopy
FEC	Fluoroethylene Carbonate
Li	Lithium
LIB	Lithium-ion Battery
Li2S	Lithium sulfide
LiCIO4	Lithium Perchlorate

LiDFOB	Lithium Difluorooxalatoborate
LiFePO4	Lithium iron phosphate
LiPF6	Lithium hexafluorophosphate
LiTFSI	Lithium bis(trifluoromethanessulfonyl)imide
NCM	Nickel Cobalt Manganese
NMP	N-Methyl-2-Pyrrolidone
OCV	Open-Circuit Voltage
PVDF	Polyvinylidene Fluoride
RF	Radiofrequency
SEM	Scanning Electron Microscope
V	Voltage
XPS	X-ray photoelectron Spectroscopy
XRD	X-ray Diffraction

List of Table and Figures

1.0 Chapter 1 – Introduction

Among the many energy storage systems, lithium-ion batteries (LIBs) are essential to human daily life, with their application gradually shifting from portable electronic gadgets to electrical Vehicles. To meet this growing demand for energy storage, lithium-ion batteries must be cost-effective, with higher energy density, less safety hazards, and longer cycle lifetimes. With considering of higher electrochemical performance, lithium-ion batteries are more desirable than other renewable energies. [1-4]. Due its low negative redox potential of -3.04 V against standard hydrogen electrode (SHE), large specific capacity 3860 mA h g^{-1}, and an elevated volumetric capacity 2060 mA h g-1, lithium metal has been regarded as best candidate for anode material. However, its draw backs include safety concerns, high cost of lithium metal, fire explosion, environmentally unfriendly, sensitive to handling in ambient temperature and other side reactions leading to dendrite growth [5] [6]. To overcome these challenges, an anode-less lithium-ion battery setup have become a popular solution route because of its distinctive benefits in preventing the accumulation of excess lithium.[7]. The anode-less battery involves only a cathode electrode, electrolyte, separator and a current collector without addition of traditional lithium metal. Therefore, the mass and volume of the lithium deposit are significantly reduced by this configuration. During plating process, lithium ions are extracted from the cathode electrode and plated on the current collector (anode electrode) as lithium metal and during stripping process, lithium are intercalated into the cathode electrode from the anode delivering a good reversibility process. [8]. Furthermore, safety hazards associated with handling of lithium metal batteries are less when compared to anode-less lithium ion battery, thus making anode-less lithium ion batteries more environmentally friendly.

However, poor reversibility of lithium-ions, high interfacial resistance between the current collector and electrolyte and capacity loss has been a major problem with anode-less batteries [9]. Generally, to achieve a higher electrochemical performance in anode-less lithium battery superior to traditional lithium ion batteries, high reversible lithium ion during charge-discharge process is required. A report from [10-12] shows that, to maintain a high capacity after 500-1000 cycles in anode-less lithium battery, 99.99% coulombic efficiency is expected and for 200 cycles, 82% CE

is also expected. Therefore, the deposition of lithium on the surface of the heterogeneous current collector and reversibility of the lithium ion needs to be uniform [13].

Herein, I have employed the use of gold sputtered 3D-CU current collector as anode electrode to substitute the traditional lithium metal in the cell configuration and NCM as the cathode material with a high concentration tri-lithium salt electrolyte.

1.1. Problem Statement

Dendrite formation in lithium-ion batteries has been a significant problem that always lead to short circuits, battery life reduction, and safety hazards. Dendrites are tiny, needle-like structures that can grow from the anode in a lithium-ion battery and penetrate the separator, and make contact with the cathode. This can lead to explosion and consumption of lithium ion. Therefore, this is a critical issue that need to be addressed to ensure the safe and efficient operation of lithium-ion batteries.

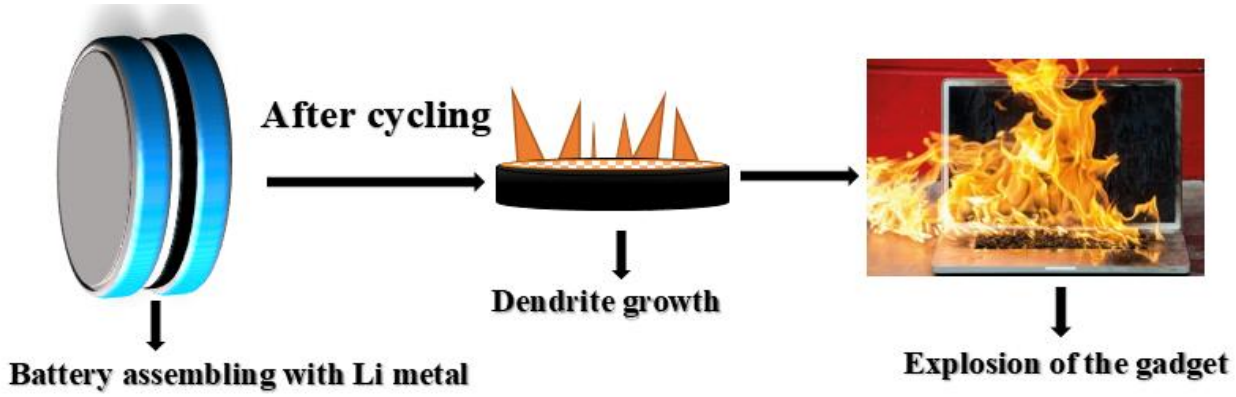

Fig 1. Research problem description.

1.2 Aim of the Research

With the strategy to minimize the effects of dendrite formation in lithium-ion batteries. This project aimed at utilizing modified three dimensional copper foam current collector and high concentration of lithium liquid electrolytes to solve the problem of dendrite formation also for the improvement of the electrochemical performance of the battery.

1.3 Objectives

- Construction of anodeless rechargeable lithium-ion battery with a suitable current collector.
- Choosing the preferred current collector as the best candidate for anode electrode material
- Achieve an excellent high and stable capacity during electrochemical performance
- Identifying and solving potential problem of dendrite formation.

1.4. Hypothesis

The hypothesis of this work focuses on the modification of the three-dimensional copper foam current collector with 50 nm thickness gold by magnetron sputtering equipment. Also, a high concentration of tri-lithium salt electrolyte will be employed.

2.0 Chapter 2 – Literature Review

2.1 Improvement strategies for anode-less batteries

Recently, many studies have been reported related to anode-less rechargeable lithium ion batteries by researchers, some of their works includes lithium-ion lost recovery, optimum reversibility of lithium-ion, electrolyte optimization and solution to interfacial problems of the current collectors with the liquid electrolyte [14] . In addition, good electrochemical performance and high energy density which are the key factors of consideration, proper optimization of the cathode material during anode-less battery construction are highly required.

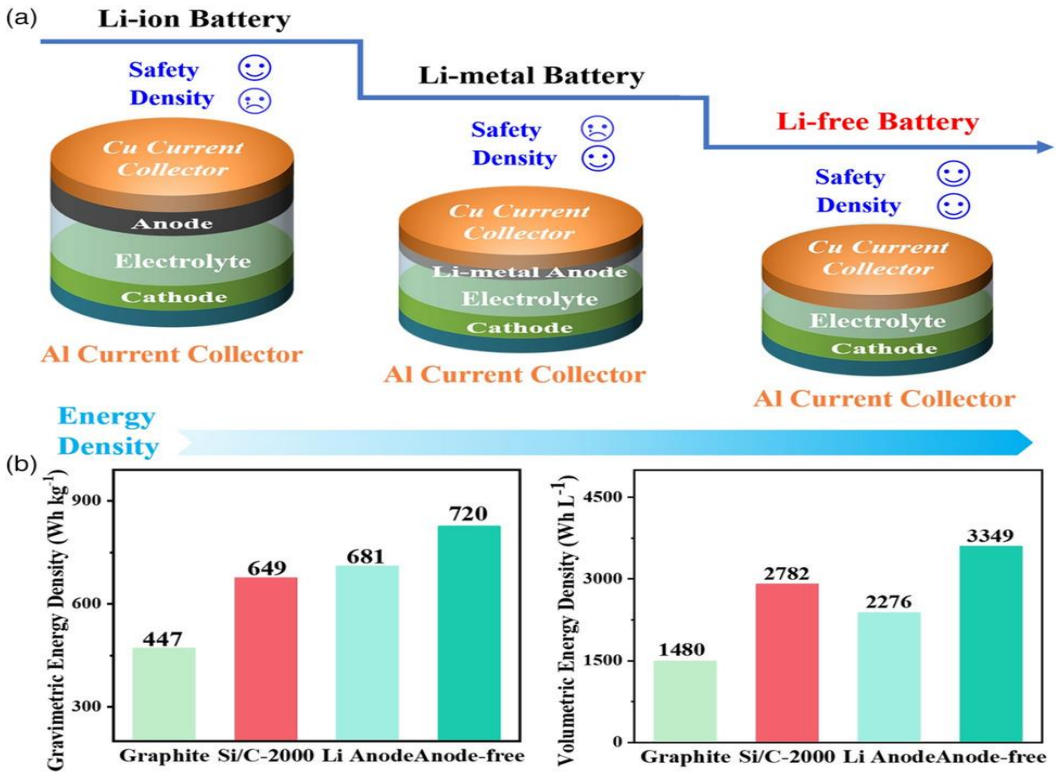

Figure 2: ***a) Schematic illustration of the full LIB, LMB and AL-IB with size and safety hazard reduction. b) Comparison of energy density of lithium metal battery and anode-less battery [18]***

Aside of the weight, safety hazard, and size reduction as shown in **figure 1,** some approaches like Electrolyte optimization, current collector modification, polymeric interfacial approach, additives methods for uniform lithium-ion flux and electrolyte solvent selection for a stable solid electrolyte interface formation have been studied [15-18] for the improvement and maintaining a high energy required in anode-less rechargeable lithium-ion battery.

2.2 Strategy on High Concentration Liquid Electrolyte Design

High concentration liquid electrolytes have been accepted as one of the enabling factor for the effective deposition of lithium in improving battery life cycle and coulombic efficiency. Also the electrolyte with unique properties passivate the lithium metal from encountering any other side reaction which may occur between the electrolyte and lithium metal. Above mentioned merits account for uniform surface morphology after cycling during charge – discharge process [19]. However, if wrong or inappropriate electrolyte design is used, there will be transport failure of lithium-ion mass through the electrolyte medium resulting in dendrite formation. Also, dendrite growth can be formed if there is non-uniform deposition of lithium-ion flux especially at the anodic electrode.

In a study, Hagos with co-workers investigated the effect of electrolytes with two different lithium salts and concentrations on anode-less rechargeable LIB. In one study, 1M of $LiPF_6$ lithium salt was dissolved in EC / DMC carbonate solvent with a ratio of 1:1 and additive of 50% volume of FEC. While the other battery construction contains 4M of LiTFSI in EC / DME in 1:2 ratio. Both the battery contains copper foil current collector as the anode electrode and was cycled with a current density of 0.2 $mA.cm^{-2}$ and starting cycling capacity of 1.7 $mAh.cm^{-2}$. After cycling, the second battery maintained a smooth morphology with a retention capacity of 60% and coulombic efficiency of 99% after 50 cycles. While the first battery had 40% coulombic efficiency and 50% of retention capacity after 50 cycles [20, 21]. This improved electrochemical Performance in the second battery is as result of high concentration of LiTFSI which offers stability of lithium deposition during cycling. In another study by Qian and co-workers, a dual lithium salt of LiPF6 and LiTFSI was dissolved in FEC / DEC solvent with the ratio 1:2, after 100 cycles the battery achieved a retention capacity of 80% with 95% coulombic efficiency. The addition of LiTFSI salt

to the electrolyte delivered uniform deposition of lithium metal during stripping and plating process with a formation of SEI yielding smooth surface of the copper foil current collector after the cycling process [19, 22, 23].

2.3 Strategies on Solvent selection for Electrolyte Design.

Apparently, one of the key factors to be considered during electrolyte design especially for anode-less battery is the choice of solvent, as solvents are very sensitive to handle especially in the immiscibility with lithium salt components. Choices of solvent for electrolyte design are mostly based on application, most commonly used solvent for electrolyte design are generally divided into two groups. The first groups are the carbonate based type of solvent which are the propylene carbonate, Dimethyl carbonate, Diethylene carbonate and ethylene carbonate. While the second group is ether based, it includes; 1,3-dioxolane and dimethyl ether [24]. Due to proven electrochemical stability and less expensive, carbonate based solvent has been used to design electrolyte particularly for lithium-ion batteries, while the ether based solvent have been greatly employed specifically for anode-less batteries because it improves the interfacial contact between current collector and the electrolyte for enabling uniform deposition of lithium on the surface of the current collector [25].

In a certain prediction made by DFT between high concentration electrolyte of 4M of LiTFSI when dissolves in DME and 1M of LiTFSI when dissolves in the same solvent, the outcomes predict that the lower unoccupied molecular orbital anions in concentrated LiTFSI salt is lower when compared to the solvent. Therefore the SEI that is very robust and inorganic rich is formed during the cycling process of charge-discharge and this SEI is majorly obtained from the salt not the solvent which helps in the lithium metal deposit at the anode [26-28]. **Fig. 2** below clearly show the wettability characteristics of high lithium salt concentration liquid electrolyte which also contribute in the uniform deposition of lithium on the surface of the anode current collector, furthermore, high lithium salt concentration offers a cathode electrolyte interface which is sufficiently inorganic and could yield a high voltage cathode operation. In the same way, high lithium salt concentration can increase the current density by delaying the lithium-ion depletion process which further suppresses dendrite growth. [29, 30].

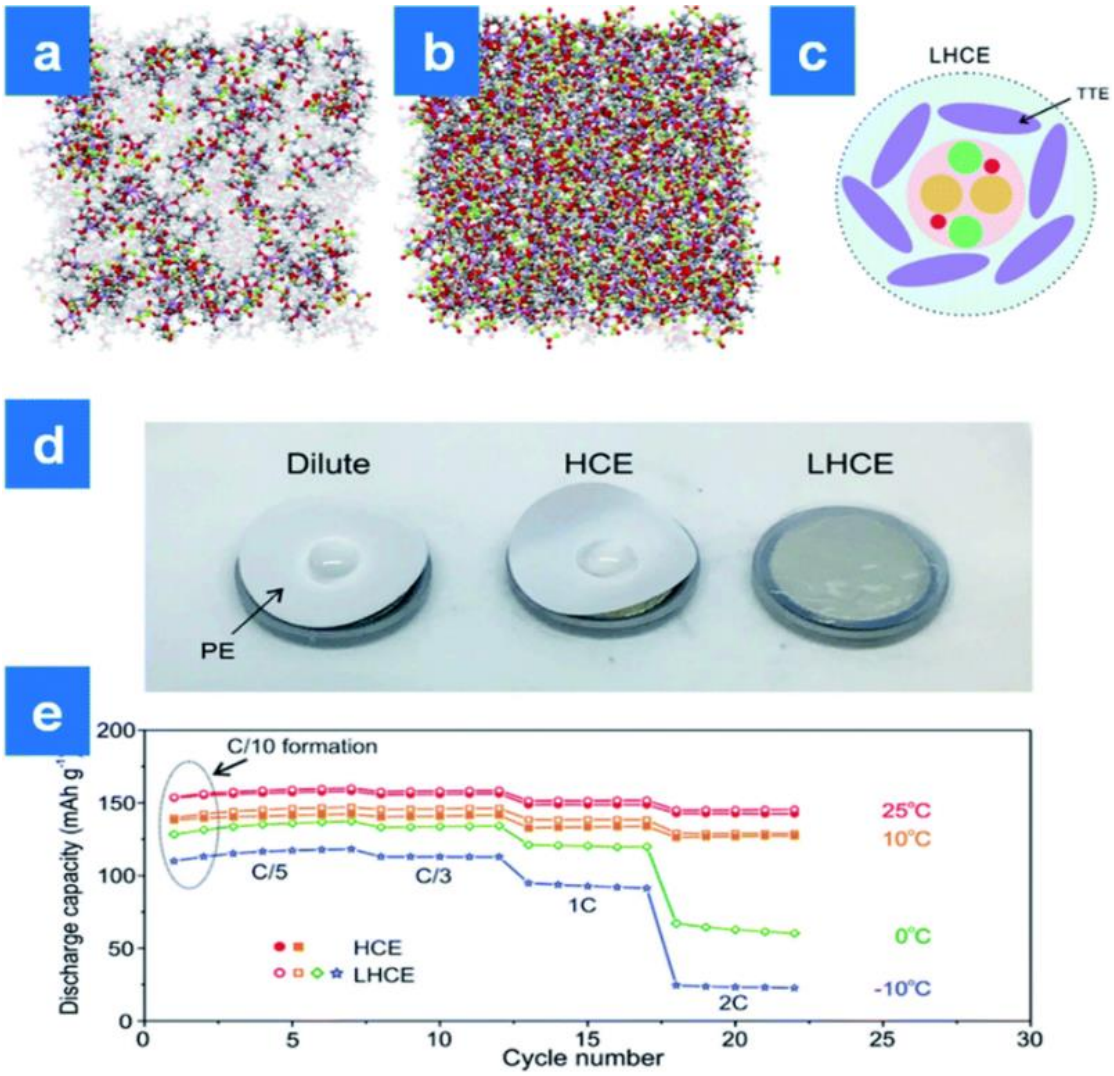

Figure 3: ***a) Schematic illustration of the cell with 1 M electrolyte, b) 4 M electrolyte, c) solvation process of LHCE, D) Wettability process with 4M electrolyte, d) the rate capability process during cycling [28]***

2.4 Modification of Current collector.

Another crucial strategy for the improvement of anode-less battery includes the modification of the current collector; the current collector plays a key role in providing a surface for the deposition of lithium during stripping and plating. Therefore, modification of the surface of the current collector improves the interfacial contact of the electrolyte and lithium deposit with morphological improvement. Many researchers have employed different ways in the modification of the current collector, which are, polymer coating, thin layer and thermal deposition of materials on the surface of the current collector [21].

A study was conducted with a current collector coated with polyethylene oxide (PEO) during construction of anode-less lithium-ion battery, the battery contains copper foil current collector as the anode electrode and LFP as the cathode with DME ether based electrolyte. After 50 cycles, the battery was to yield 64% retention capacity and almost 90% coulombic efficiency. Another study was also done, this time the improvement of the electrochemical performance was the aim, in this study a combination of thin lithium and tin layer was carefully deposited on the surface of the bare copper current collector. Carbonate based electrolyte of LiPF6 was added to the battery construction, after 50 cycles the cyclic performance was increased by 50% and retention capacity to 30% [31, 32].

Furthermore, a 3D host current collector has been constructed to investigate the lithium deposit for the anode-less lithium ion battery. The nucleation Overpotential and current density of the metallic 3D current collector rises during electrodeposition of lithium, because the lithium nuclei is not directly the same as the nucleation Overpotential, therefore the particle size of the lithium deposit increases with low current density which can lead to other side reactions. Another important information to consider, the 3D metallic host current collector offers a wide surface area for nucleation sites especially for uniform and smooth deposition of lithium, thus could help confine the lithium deposit into the metallic 3D pores. However, the interfacial contact between the electrolyte and the 3D host current collector is lower than that of bare current collector [33].

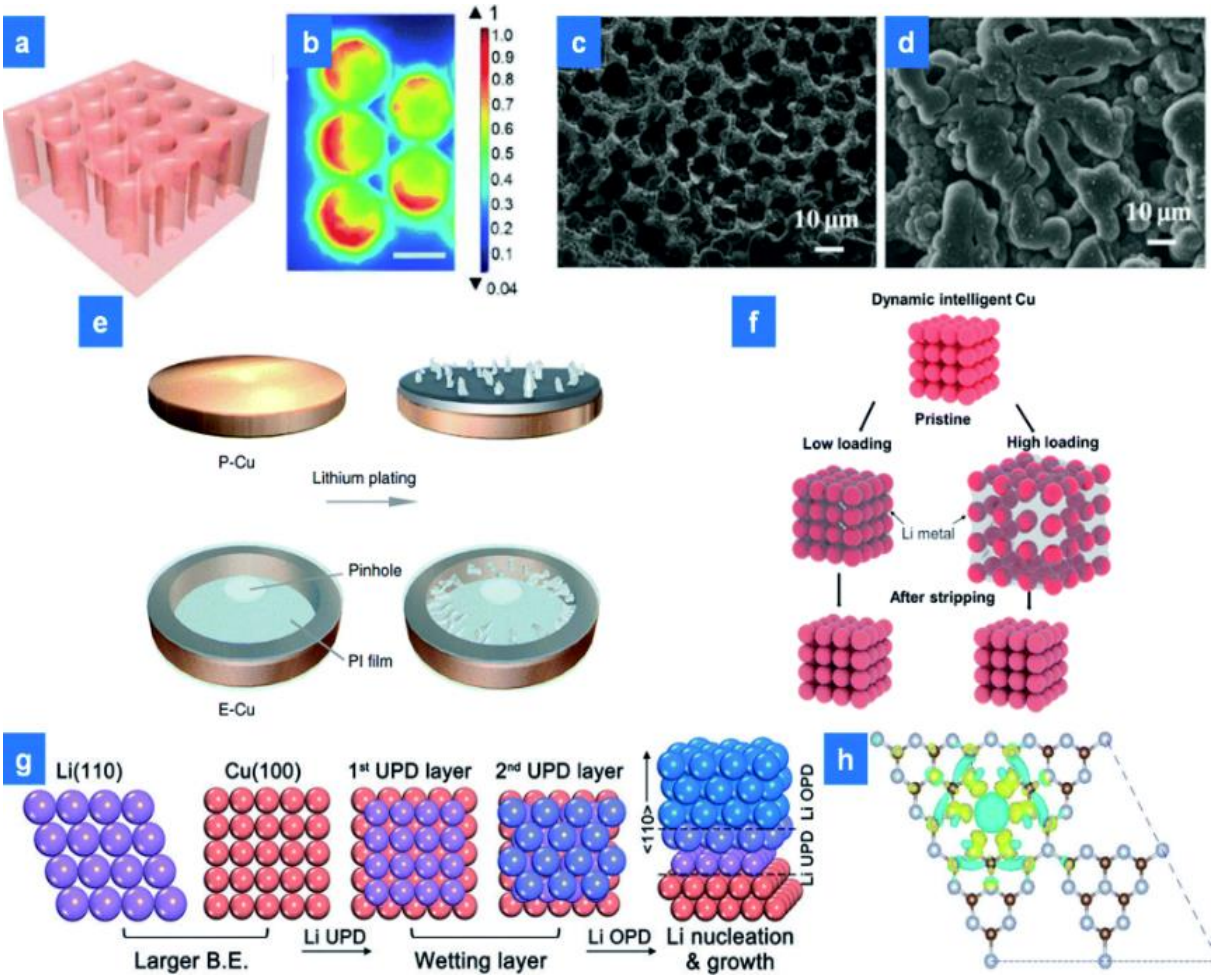

Figure 4: ***a) Schematic illustration of the cell with 1 M electrolyte, b) 4 M electrolyte, c) solvation process of LHCE, D) Wettability process with 4M electrolyte, d) the rate capability process during cycling [36]***

According to **fig. 3**, which illustrates different types of 3D host structure of current collector, **fig. 3g** a rigid porous and expandable 3D current collector specifically was compared, during cycling process, rigid porous current collector exhibit a stable lithium deposit during stripping and plating, although some demerit can arise from the handling of large amount of lithium deposit with limited surface area for stripping and plating process. On the other hand, **fig. 3f**,

expandable 3D host current collector has offered more surface area with safe handling of high or excess lithium deposits, these advantages can be possible due to the expandability property to accommodate volume expansion of lithium deposition. However, the slow stripping and plating process which increase the time of cycling also increase the energy barriers to overcome for the complete stripping and plating process[34, 35]

2.5 Additives methods for uniform lithium-ion flux distribution.

Additives have been adopted as another strategy for the improvement of electrochemical performance of anode-less lithium ion battery. Addition of additives in liquid electrolyte during anode-less battery construction helps to provide uniform distribution of lithium –ion flux on the surface of current collector during stripping and plating [36, 37]. Self-healing and seeding additive configuration have been commonly used by many researchers and have obtained a homogenous deposition of lithium and Cs^{+} especially at lower concentration with a reduced potential lower than Lithium-ion which has maintained Lithium-ion reduction throughout the process [29, 38, 39]. According to **fig. 4a and b,** we can observe that the protruded part of the lithium deposition absorbed Cs^{+} because these are the high space charge zone, which electrochemically covers the negative charges and has not been reduced. It's also observed that while the negative charges were disappearing the lithium ions were not able to get to the tip of the lithium deposit thereby hindering future protrusion while uniform lithium ion flux distribution was maintained. In **fig. 4c.** It has been approved that lithium-ion has great affinity with Nano diamonds particles of sizes lower than 500 nm. Therefore as an additive, when these Nanodiamond particles are spread in the electrolytes, the lithium –ion tends to be attracted by the Nanodiamonds particles [40]. By absorption of lithium-ion by Nanodiamonds, the lithium deposit distribution becomes uniform without any protrusion growth on the surface of the current collector.

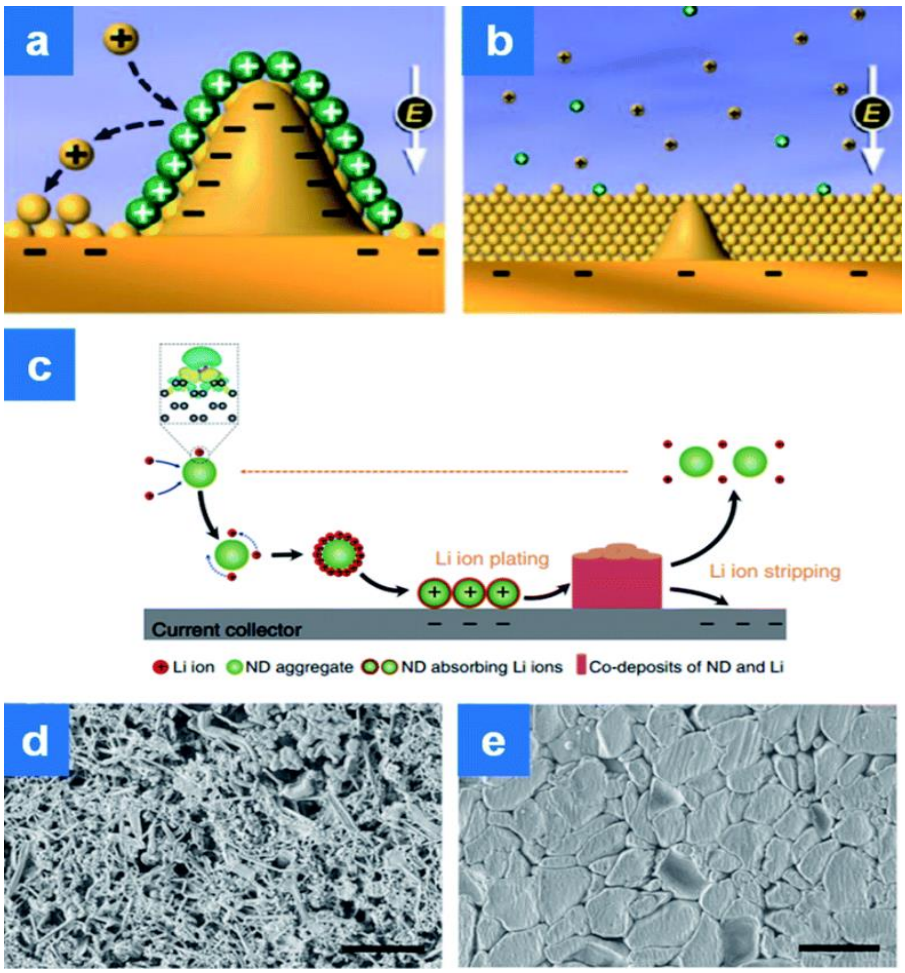

Figure 5*: a) protrusion of lithium deposit with Cs+ aligned round, b) diminishing process of the protrusion of the lithium deposit, c) effect of Nano diamonds particle in liquid electrolyte, D) surface morphology of current collector without NDp, d) surface morphology of current collector with NDp [40]*

Fig 4d and e are the SEM images comparing the difference between the effects of lithium deposit on the surface of current collector when Nano diamonds are added in the electrolyte and when the Nanodiamonds are absent. It can be seen that in fig. 4d, the lithium deposition has some protrusion part while fig. 4e has a smoother surface of lithium deposit because of the effect of Nanodiamonds addition In the electrolyte [41].

2.6 Recent works on Anodeless Batteries.

2.6.1 Anode-less Li_2S battery with thin film gold on 2D-Cu current Collector

In this Study, the fabrication of anode-less lithium sulfur battery with bare copper current collector as the anode electrode was used. This work evaluates the effect of lithium deposit on gold modified copper current collector by suppressing dendrite growth, the thin layer gold on the surface of the copper current collector helps to reduce the nucleation barrier during lithium deposition and not reducing the energy density in the process. The full cell consist of Au@2D-CC || Li_2S where the bare copper is the current collector for anode and aluminum foil for Li_2S as the cathode with LiTFSI in DOL/DME 1:1 electrolyte [42].Both cell were cycled for first charge and discharged at a cut off voltage of 1.7V and 3.8V at a 0.05C with addition of 30 µL.The electrochemical evaluation and post mortem analysis from **fig. 6** shows the result after the cycling process of the battery**. Fig.6a and b** illustrate the first charge of both bare copper current collector and copper current collector with gold membrane which are approximately 1100 mAh g-1 and 1000 mAh g-1 capacity respectively while **fig. 6 b-h** shows the surface and cross sectional morphology of both batteries after first charge. The battery with gold copper current collector has a smooth surface of lithium deposit after first charge which allows a stable SEI.

Fig. 6 i and m also illustrate the first discharge of both battery with bare copper and gold modified copper current collector with capacity of approximately 650 mAh g-1 and 750 mAh g-1 respectively, it is very clear to see that discharge capacity with gold modified copper current collector is high compared to the bare copper current collector. This improvement is due to the effect of modification of the CC by gold membrane which allows the uniform transportation of lithium-ion during stripping and plating. Also the SEM images from fig.6 j –p shows the morphology structure after first discharge. Due to the lithiophilic nature of the gold modified CC, the thickness deposition of lithium metal is lesser in contrast to bare CC [42]

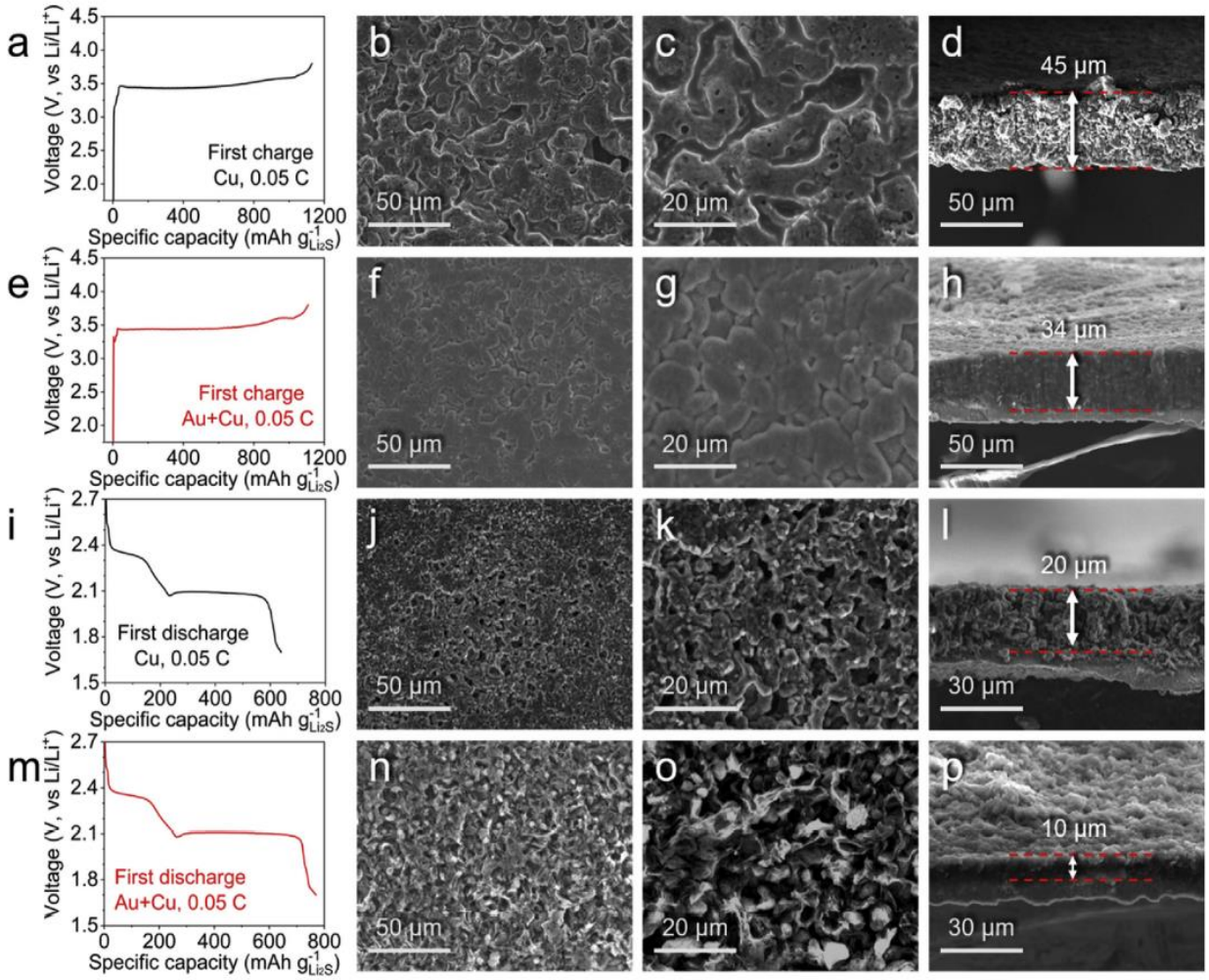

Figure 6*: a-m) first charge-discharge after stripping/plating, b-h) SEM images after first charge lithium deposition with cross section images, j-p) SEM images of deposited lithium after first discharge with corresponding cross section images. [41]*

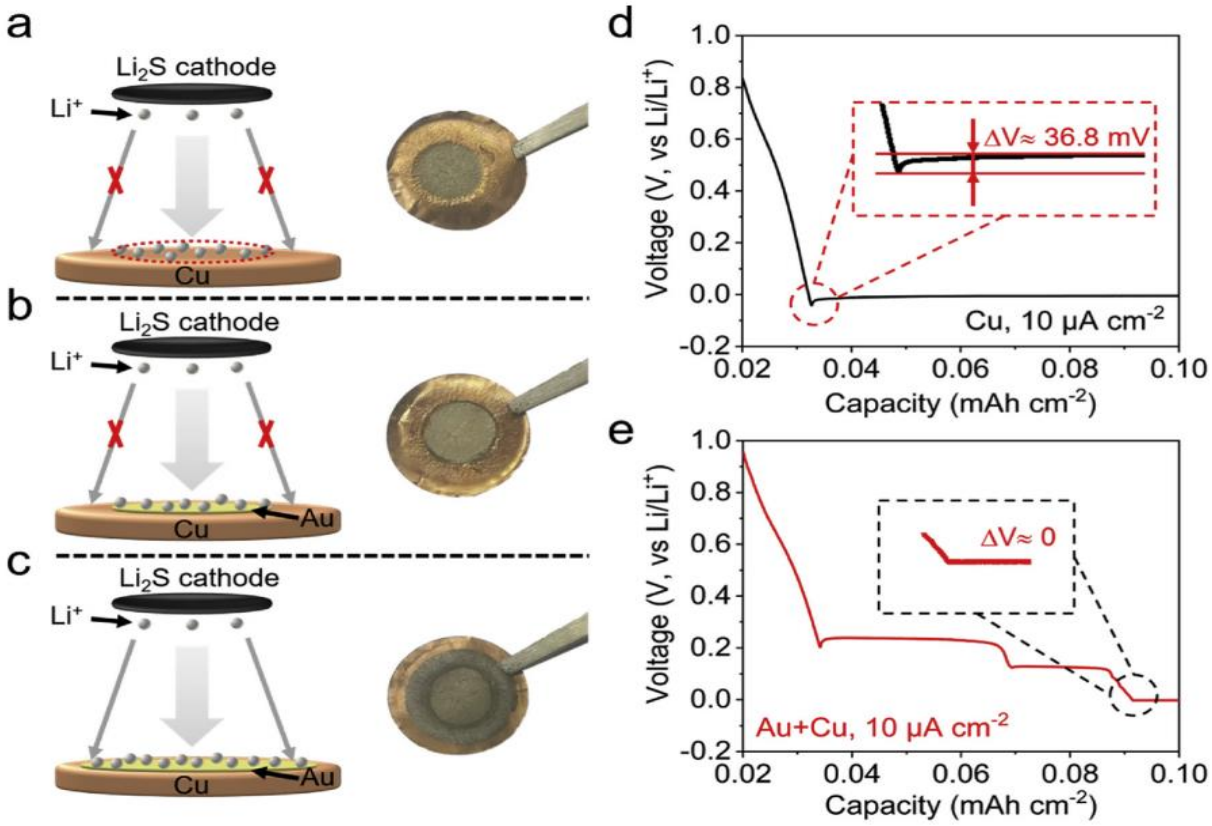

Figure 7: ***effect of lithium deposit on (a).bare and (b). Coated copper current collector [42].***

2.6.2 Graphene modified 3D-Cu current Collector

In another study, Juan Yu et, worked on a graphene-Modified 3D copper foam current collector for Dendrite-free lithium deposition. In this study, the aim was to examine the property of the rO3D-Cu as a substitute to the commercial copper foam. For a clearer result, the experiment was conducted between rO3D-Cu, 3D-CU and 2D-cu foil half-cell with lithium metal as a reference electrode. After cycling process, the dendrite formation was lesser in 3D-Cu battery compared to dendrite formation on 2D-Cu battery while rO3D-Cu shows no dendrite formation do to the modification of 3D-Cu with reduced graphene oxide as illustrated in **figure 8** [43].

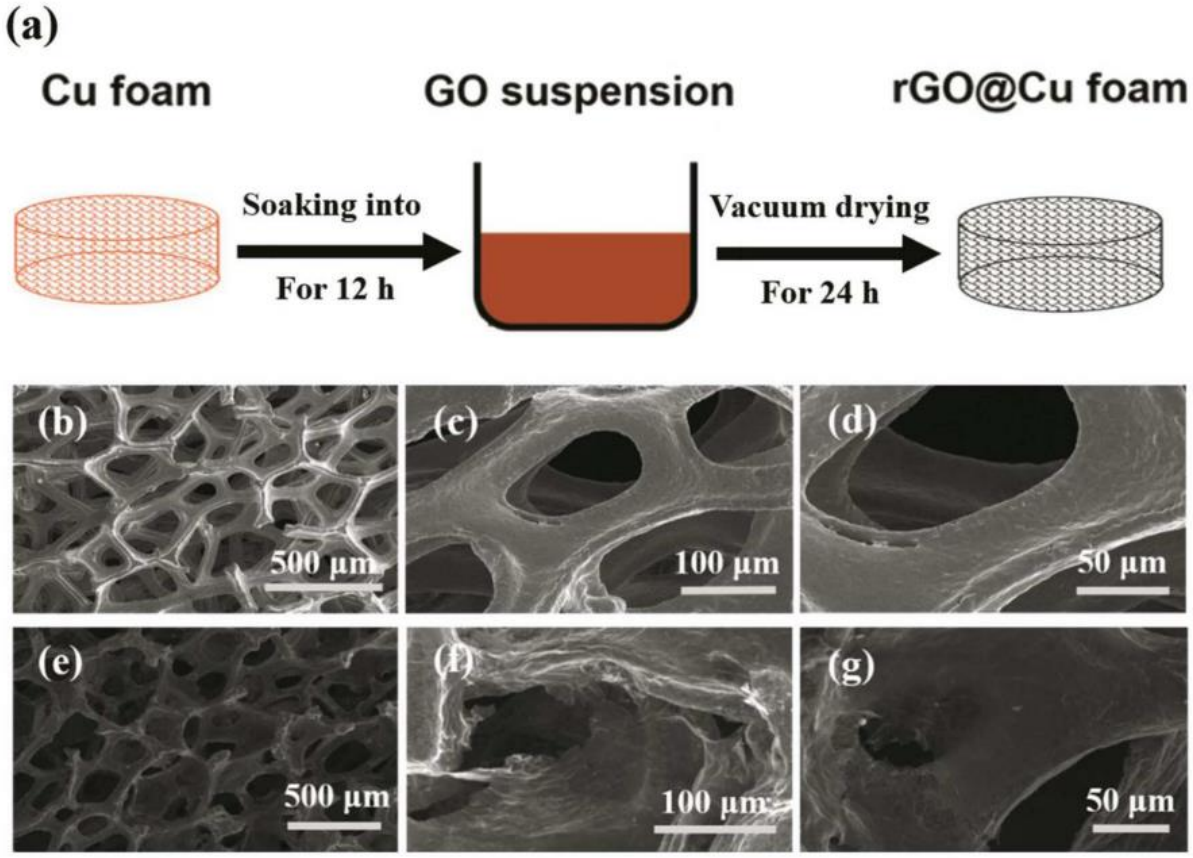

Figure: 8 ***(a) Modification process of the 3D-Cu foam to rO3D-Cu foam. (b-d) shows SEM image of the 3D-Cu foam before modification. (e-g) demonstrate the SEM image of the 3D-Cu foam after modification with graphene Oxide*** *[43]*

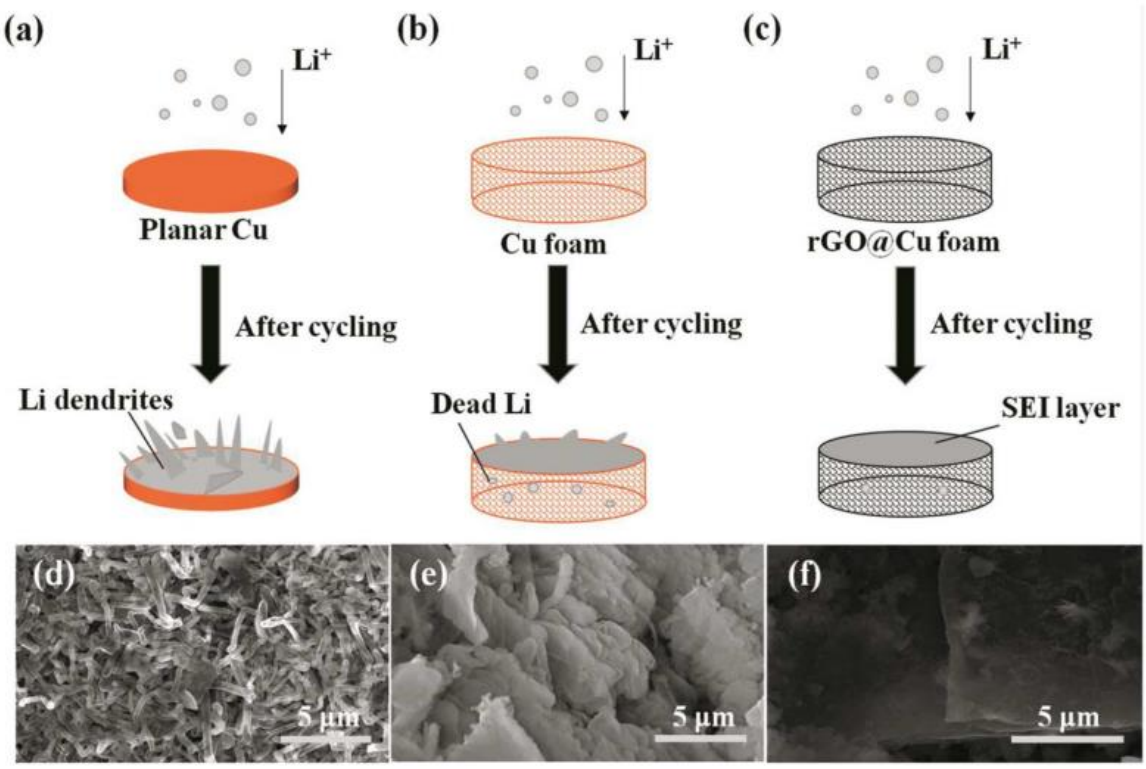

Figure: 9 ***schematic diagram of lithium deposit. a).2D-Cu with lithium deposit, b). 3D-Cu with lithium deposit, rGO3D-Cu with lithium deposit and SEM images of the lithium deposit across the different CC. [46]***

Also, the electrochemical performance of the three different batteries was examined with a lithium metal chip as reference electrode, the batteries were cycled for about 4 times to remove surface impurities in other To form SEI with starting voltage of 0-5V and current density of 50 µA. The battery was later cycled for different times of cycles from 10^{th} – 300^{th} times as shown in **fig. 9.a - d.** After 10^{th} cycles, the 2D-Cu and 3D-Cu show a very high discharge plateau with a reduced charge voltage plateau more than the modified CC. This significant change can be explained that the graphene modified CC, was not been fully activated by the presence of the liquid electrolyte, but another sharp observation was made after the 100^{th}, 150^{th} and 300^{th} cycles, at this point, the graphene modified CC achieved both higher charge and discharge voltage plateau in

contrast to the lower charge and discharge voltage plateau of the other cell. Furthermore, this second change was as a result of high lithium deposit on the 2D-Cu and 3D-Cu CC which leads to capacity decay and irreversibility of Li deposition. While the graphene modification on the 3D-Cu CC helped to maintain uniform lithium deposition and a stable SEI [43]

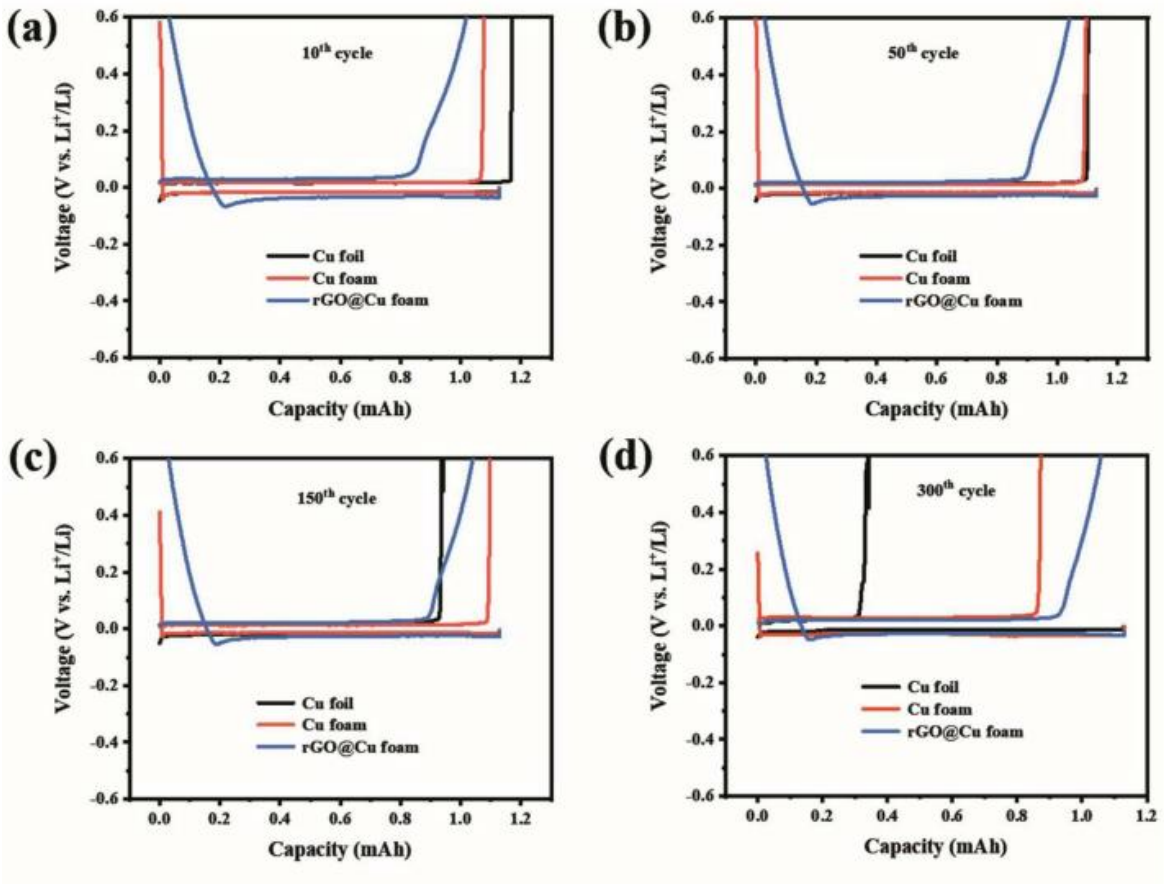

Figure: 10 ***schematic diagram of lithium deposit. a).2D-Cu with lithium deposit, b). 3D-Cu with lithium deposit, rGO3D-Cu with lithium deposit and SEM images of the lithium deposit across the different CC.[44]***

In the further investigations, the above mentioned copper electrodes, were also used to assemble a full cell battery as anode while $LiFePO_4$ served as the cathode materials as shown in **Fig. 10a**, the assembled full cell batteries were galvanostatically measured from 2.0-4.4V at 1C.

The 2D-Cu full cell is observed to maintain a capacity of 132 mAh/g at first cycle while drastically reduced to 57.6 mAh/g after about 15 cycles achieving a coulombic efficiency of 41%. This was as a result of lithium metal depletion and forming dendrite on the surface of the copper electrode which reduces the battery capacity and leads to dead battery. In contrast, full battery assembling with 3D-Cu electrode and $LiFePO_4$ maintained about 132.9 mAh/g at first cycle and partially reduced to 126.2 mAh/g after more than 200 cycles with a stable coulombic efficiency of 64%. Finally, the modified rO3D-Cu with $LiFePO_4$ delivered a steady cycling of 135 mAh/g capacity with a coulombic efficiency of 80%. The full cell of modified graphene 3D-CC exhibited steady lithium deposit with capacity depletion. This means that modified copper electrodes can not only subdue dendrite formation but can also maintain high capacity during battery operation with a good coulombic efficiency which always improves battery lifecycle. **Fig. 10b** demonstrates the rate performance of all these different types of copper electrodes mentioned above with different current densities. The rate capability of these batteries was also investigated under different C-rates within above 5 cycles. At 0.5 C, it was clearly seen that there was 100 % coulombic efficiency which causes capacity decay when the current density is increased [44].

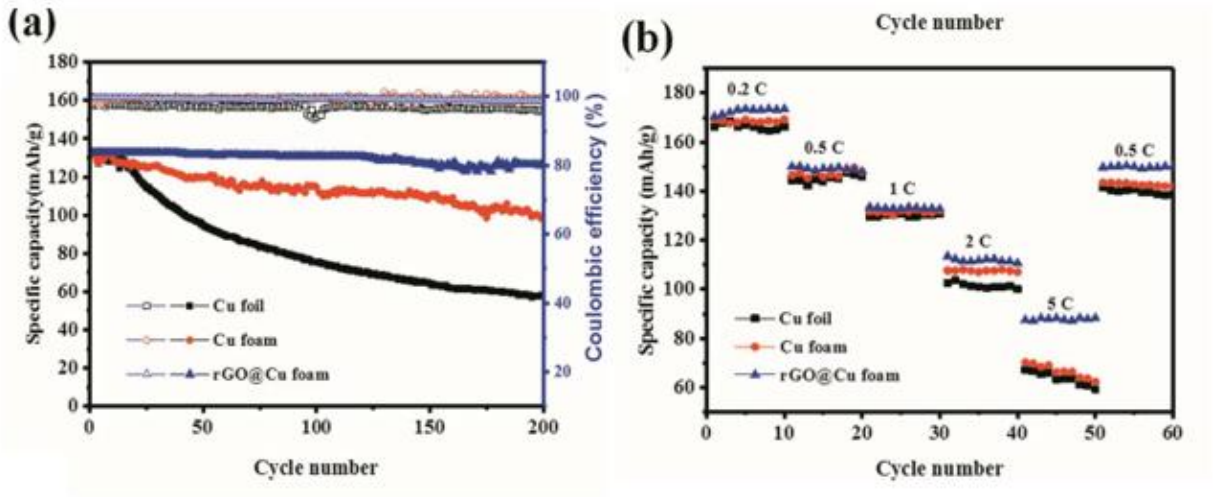

Figure: 11 ***schematic diagram of lithium deposit. a).2D-Cu with lithium deposit, b). 3D-Cu with lithium deposit, rGO3D-Cu with lithium deposit and SEM images of the lithium deposit across the different CC. [44]***

3.0 Chapter 3 – Materials and Methods

3.1.0 Anodeless battery construction

The commercially available copper current collectors (2D, 3D) with a thickness of 0.01 mm and 0.11 mm respectively, were carefully punched to a diameter of 14 mm and thoroughly cleaned 3 times with ethanol and acetone (v/v 1:1) in an ultrasonic bath equipment for about 30 mins to remove contamination and impurities that might be trapped on the surface. The current collectors were dried in a vacuum oven at 80 ^{0}C for about 30 mins to remove the traces of organic solvent. The 2D, 3D current collectors were modified by sputtering 50 nm and 100 nm thickness of gold on the surface of the 2D, 3D current collectors and prepared as anode electrode as shown **Fig. 11** below. Also, it is important to mention that sputtering of 100 nm thickness of gold on the CCs was compared with 50 nm, which the later gave an excellent result. The sputtering parameters are clearly shown in the **table 1** below.

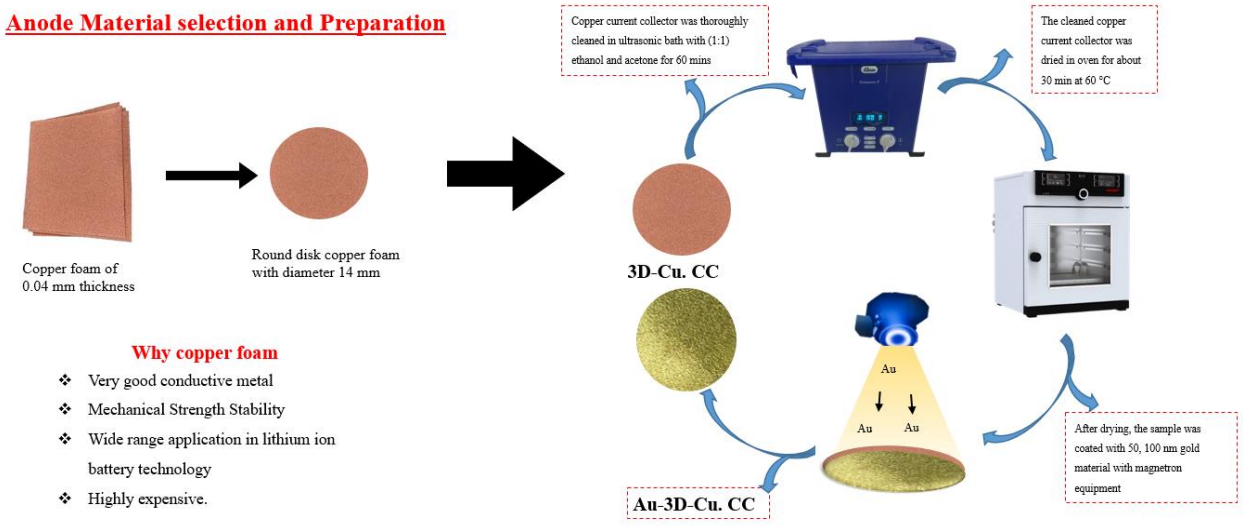

Figure 12: ***Preparation process of copper current collector material***

Table 1; ***sputtering parameters for the modification of copper current collectors***

Equipment	Target Material	Material sputtered on:	Thickness	Sputtered Pressure	Gas Power	Rotation Speed	Observation
RF Magnetron Sputter	Gold (Au)	2D- Copper (Cu)	50 nm	5m Torr / 15 sec	Argon	10 rpm	Good Result
RF Magnetron Sputter	Gold (Au)	2D- Copper (Cu)	100 nm	5m Torr / 15 sec	Argon	10 rpm	Poor Result
RF Magnetron Sputter	Gold (Au)	3D- Copper (Cu)	50 nm	5m Torr / 15 sec	Argon	10 rpm	Good Result
RF Magnetron Sputter	Gold (Au)	3D- Copper (Cu)	100 nm	5m Torr / 15 sec	Argon	10 rpm	Poor Result

3.1.1 Half-cell construction with bare 2D copper foil, and 3D copper foam current collector.

After the copper current collector was prepared, a half-cell battery was constructed with lithium metal, bare copper current collector and modified copper current collector as the anode with $LiPF_6$ electrolyte and polypropylene separator. The aim of this half-cell was to investigate the deposition effect of lithium metal and the ability of the different copper current collectors to host the lithium deposit. The stripping and plating process of the half-cell is represented in **Fig.12a and b.** as 2D-Cu || Li and 3D-Cu || Li, and Au-2D-Cu || Li and Au-3D-Cu || Li after modification which is represented in **Fig. 12c and d.**

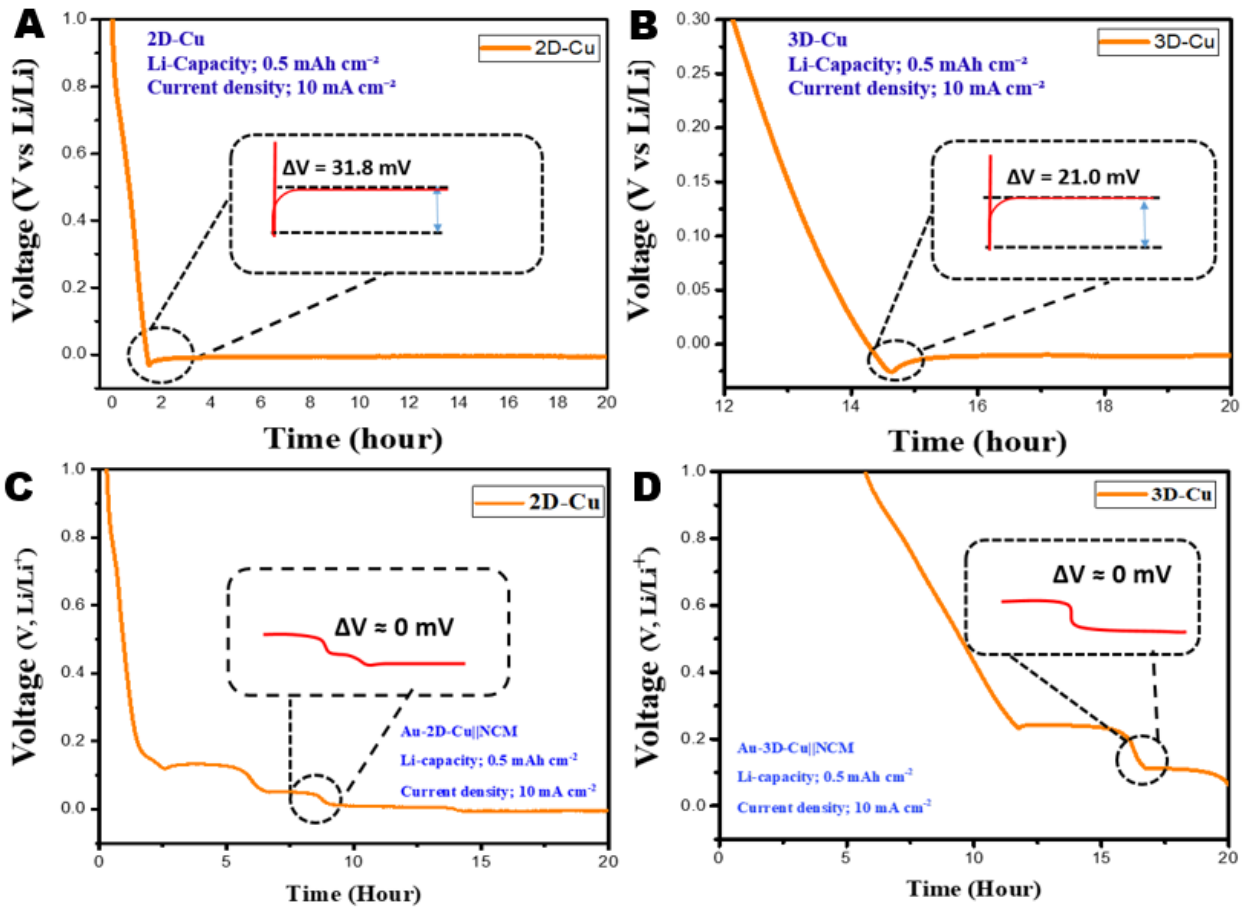

Figure 13: ***stripping and plating process. a) Bare copper with lithium metal (2D-Cu || Li.). b) Copper foam with lithium metal (3D-Cu || Li). c) Modified bare copper with lithium metal (Au-2D-Cu || Li). d) Modified copper foam with lithium metal (Au-3D-Cu || Li.)***

3.1.2 Cathode electrode preparation

The overall electrode preparation procedure is**.** Firstly, the cathode powder was dried for about 30 mins at 80^0C to remove trapped moisture content. During slurry preparation, PvDF was thoroughly dissolved in 1 ml of 98% of NMP organic solvent with thinky mixer at 2000 rpm for 15 mins, the active material was added with the consequent mixing for another 15 mins followed by the addition of conductive material with additional 1 ml NMP for the last 15 mins to obtain a homogenous mixture of slurry formulation as depicted in **Fig. 13**. The cathode materials includes; 88.5% NCM (Active Material), 6.5% carbon black (Conductive Material) and 5% (PvDF) Polyvinylidene fluoride (binder material). The prepared slurry was casted on an already cleaned aluminum foil with the help of doctor's blade and dried for 24 hours in a vacuum oven overnight to remove the organic solvent. After drying, the dried electrode with thickness of 0.25 mm was carefully punched into a round disc of 14 mm diameter and was transferred into the argon-filled glove box ready for battery assembling.

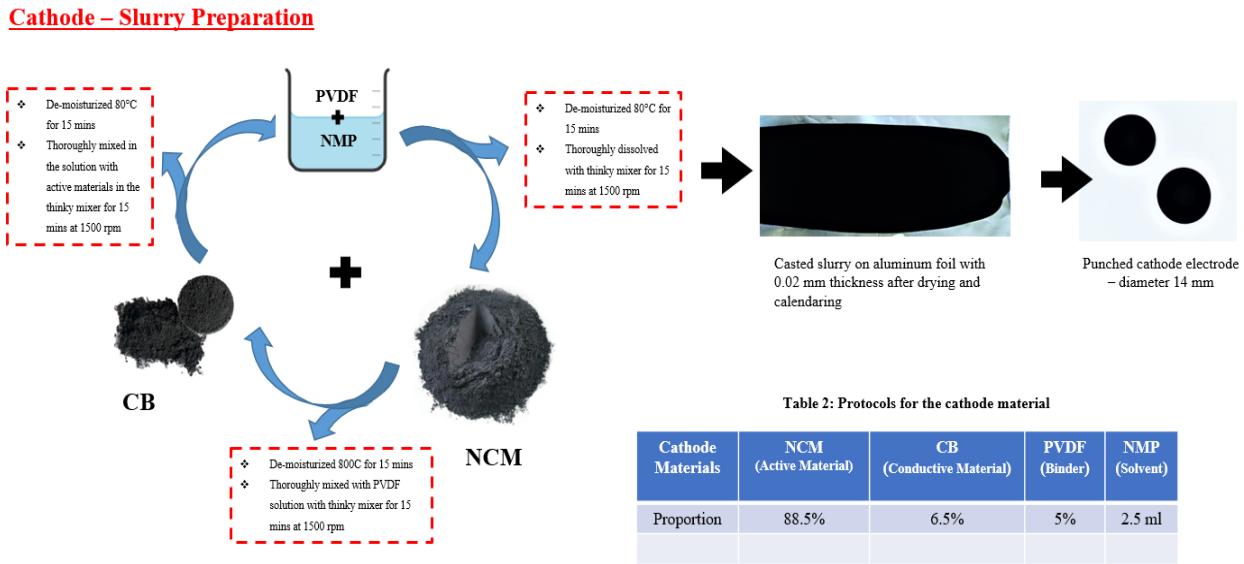

Table 2: Protocols for the cathode material

Cathode Materials	NCM (Active Material)	CB (Conductive Material)	PVDF (Binder)	NMP (Solvent)
Proportion	88.5%	6.5%	5%	2.5 ml

Figure 14*; Cathode electrode preparation process.*

3.1.3 Full-cell with modified 2D copper, 3D copper foam current collector with NCM.

In the full-cell configuration, the modified copper current collectors were used as an anode electrode as (Au-2D-Cu || NCM) and (Au-3D-Cu || NCM) while NCM ($LiNi_{1/3}Co_{1/3}Mn_{1/3}O_2$) was used as the cathode electrode. 1M $LiPF_6$ in EC/DMC (1:1 v/v) was used as the liquid electrolyte and polypropylene as the separator. The full-cell was assembled in the glove box with less than 0.1 ppm for both oxygen and water, the OCV of the full cell showed 0.3 due to limited lithium metal in the cathode electrode.

3.1.4 Materials Characterization.

The surface of the copper current collectors were analyzed using the scanning electron microscopy (SEM, JSM-7500F JEOL, Japan), coupled with energy-dispersive X-ray spectroscopy (SEM-EDS, USA) for the analysis of elemental distribution. X-ray diffraction (XRD, SmartLab. Co., Japan, Cu Kα radiation, $\lambda = 0.154056$ nm) was employed to investigate the structure with a 2θ range from 20 to 80 ^{0}C at a scan rate of 6 degrees / mins with the help of 40 KV, 30 Ma X-ray as shown in **Fig. 15** below.

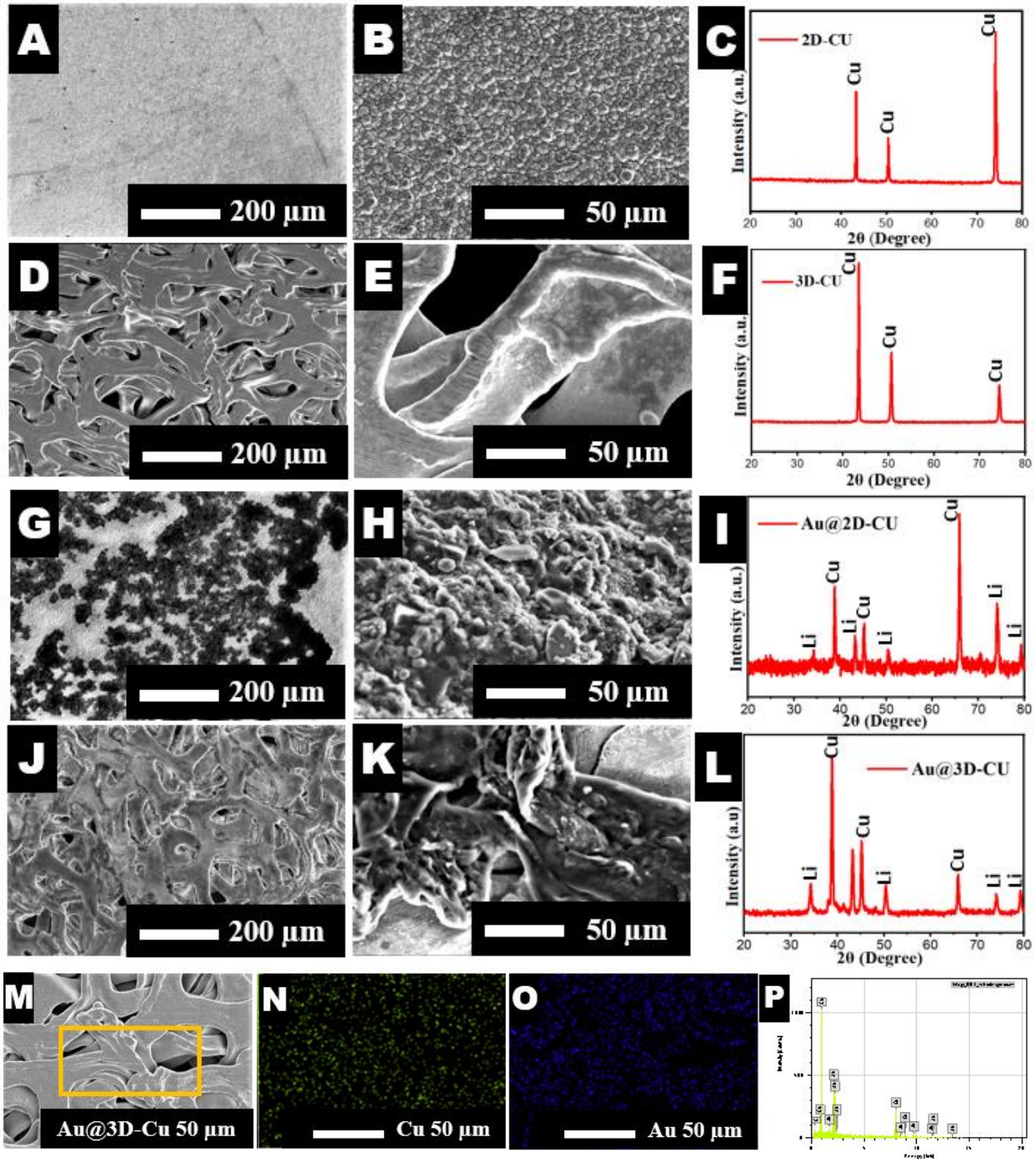

Figure 15; (a, b, c, d, e, f.) SEM images and XRD of bare copper and copper foam before sputtering, (g, h, I, j, k, l) SEM images and XRD of modified copper current collectors after lithium deposition, (m, n, o, p) EDS elemental mapping of the copper current collectors after gold sputtering modification.

Fig. 15a, b, d and e. illustrate the SEM images of bare copper foil and bare copper foam before lithium deposition. From the images we can observe that the bare copper foam has pores which makes it have more surface area than the bare copper foil. XRD analysis of bare copper foil and foam are depicted in **Fig. 15 c and f.** showing that there is no changes in the peaks of the bare copper foil and foam, while **Fig.15 g, h, j, and k** clearly illustrate the deposition of lithium on the surface of the modified copper foil and copper foam before modification of the CCs. Due to the uneven deposition, there are many protruding lithium deposits on the surface of Au-2D-Cu current collector but few protuberances of lithium were observed on the surface Au-3D-Cu copper current collector because of the excellent distribution of Au layer because of lithiophilic characteristics. Therefore, SEM images correspond with the voltage profiles after the current collectors' modification. Furthermore, the XRD analysis after lithium deposition in **Fig. 15 i and l** show that that the only difference at the peaks is the presence of lithium metal on the surface of the current collectors, while **Fig.15 m, n, o, and p** illustrate the elemental mapping of gold material on the surface of the bare copper foil and copper foam indicating good crystallinity of the gold material on the surface of CCs.

4.0 Chapter 4 – Result and Discussion

4.1 Electrochemical performance evaluation

In **Fig. 12 a and b** above, the stripping and plating processes were cycled on time dependent per hour with a lithium deposit capacity of 0.5 mAh cm^{-2} and a current density of 10 mA cm^{-2}. The overpotential value with a bare 2D-Cu foil current collector showed 31.8 mV, while a bare 3D-Cu foam current collector maintained an overpotential value of 21.0 mV. The reduced overpotential value with a bare 3D-Cu current collector could be attributed to the porous scaffolding of the structure, which allowed for more surface area. In a second cycling, modified Au-2D-Cu and Au-3D-Cu current collectors with the same parameters as mentioned above showed overpotential values of 0 mV and 0 mV, respectively, after cycling, as shown in **Fig. 12 c and d** above. This result explained the effectiveness of the sputtered gold crystalline on the surface of the copper current collectors in stepping down the local current and making the current collectors lithiophilic materials for hosting lithium deposits. For further electrochemical investigation, a full-cell with NCM cathode electrode and modified copper current collectors was constructed as mentioned in the experimental section above.

Cyclic voltammetry analysis was conducted using a BioLogic tester VMP3 Science instrument with a potential range of 2.5 – 4.5 V for Au-2D-Cu || NCM and Au-3D-Cu || NCM (vs. Li^+/Li) with a scanning rate of 0.1 mV s^{-1}. During the scanning process, both Au-2D-Cu || NCM and Au-3D-Cu || NCM experienced a rough scanning at the beginning of the scanning process which correspond to the activation of the NCM with the liquid electrolyte and later normalized as the scanning continued with oxidation and reduction peaks of Au-2D-Cu || NCM maintained at 4.0 V, 4.1 V || 3.9 V,4.0 as shown in **fig. 16b** while in **fig. 16c** the Au-3D-Cu || NCM oxidation and reduction peaks occurs at 3.9 V, 3.7V || 3.8 V,3.7 which is similar to the traditional electrochemistry of NCM with lithium metal as shown in **fig. 16a**

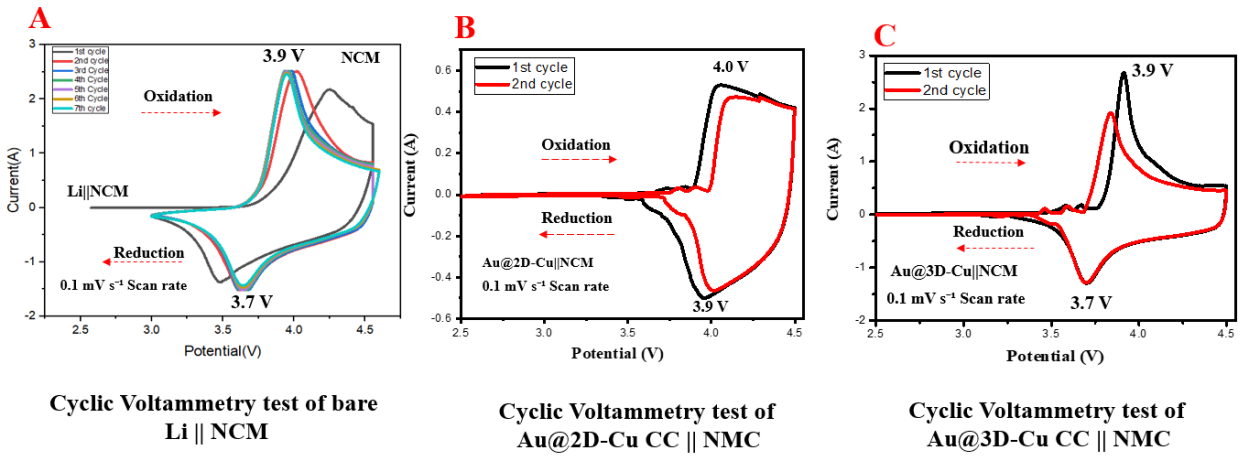

Cyclic Voltammetry test of bare Li || NCM

Cyclic Voltammetry test of Au@2D-Cu CC || NMC

Cyclic Voltammetry test of Au@3D-Cu CC || NMC

Figure 16*: Cyclic voltammetry performance of a). Lithium metal with NMC battery, b.) Au-2D-CC with NMC battery and c). Au-3D-CC with NMC battery.*

4.1.1 Charge-Discharge with $LiPF_6$ Liquid Electrolyte

The first set of full cells was initially assembled with 1M of LiPF6 in EC/DDEC carbonate solvent (1:1 v/v) as 3D-Cu || NCM, Au-2D-Cu || NCM, and Au-3D-Cu || NCM, as shown in **fig. 17.** It was cycled at 0.2 C, and traditional lithium metal with NCM was also assembled to compare the charge-discharge of the anode-less, as shown in **Fig. 17a.** The first charge of Au-2D-Cu || NCM in **Fig. 17b** showed above 200 mAh g-1 in the first cycle, which corresponds to the activation of NCM with electrolyte. After 3 cycles, the capacity drops to 115 mAh g-1 with a CE of 77%; however, the capacity keeps dropping as the battery keeps cycling. This capacity decay was because LiPF6 electrolytes only assured high capacity but poor lithium stability during stripping and plating. In **Fig. 17c,** the 3D-Cu || NCM showed a first charge of almost 200 mAh g-1 with 110 mAh g-1 of discharging capacity, giving a CE of 76%. After 3 cycles, the capacity decay was more obvious than with the Au-2D-Cu || NCM. In Au-D3-Cu || NCM, a high capacity was achieved at 160 mAh g-1 and a discharge capacity of 110, giving a CE of 84 %, while the capacity decay kept dropping as the cycling continued. Due to the limited presence of lithium metal, the reversibility of lithium-ion with the electrolyte was poor for all the charge-discharge processes in all the cells. To improve the stability of the lithium-ion battery, high concentrations of electrolyte were employed for this purpose.

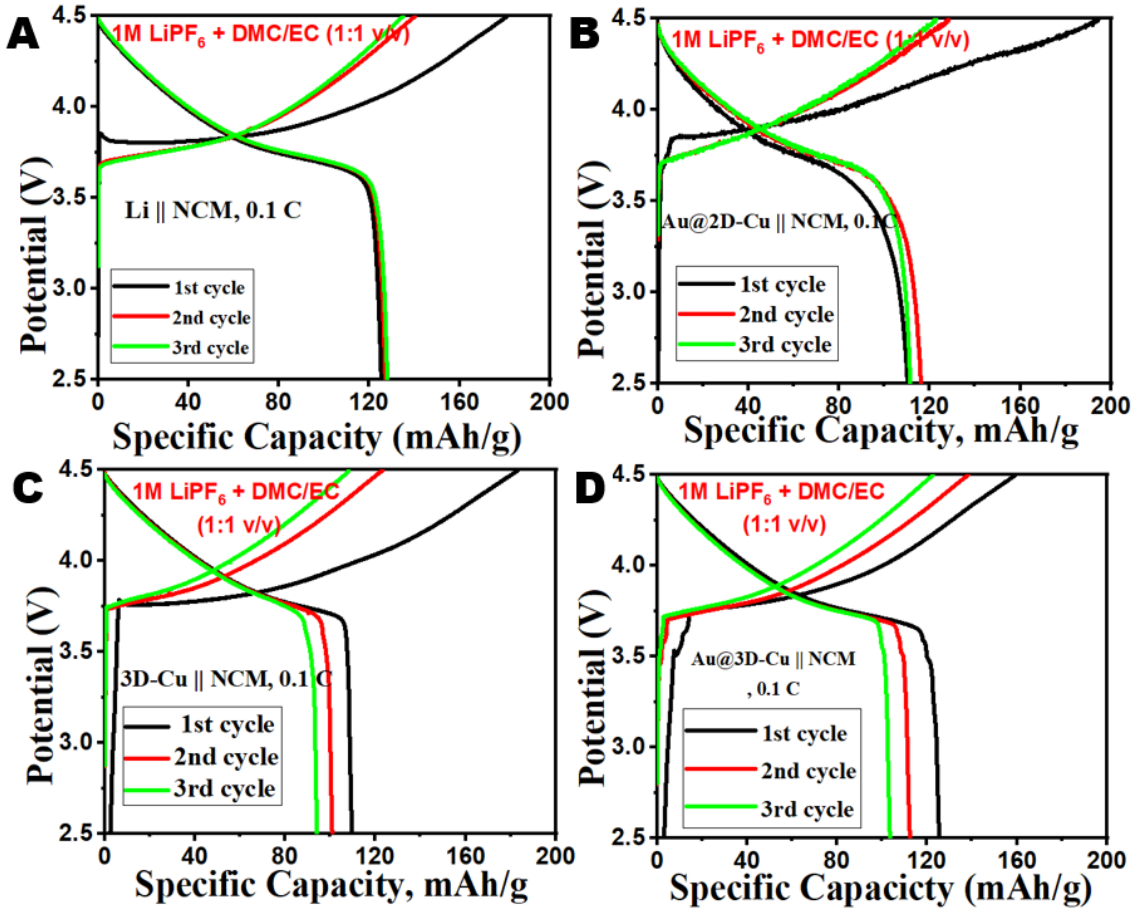

Figure 17; first charge-Discharge profile with $LiPF_6$ liquid electrolyte a). Charge-Discharge profile of Li // NCM, b.) Charge-Discharge profile Au-2Cu // NMC c.) Charge-Discharge profile 3D-Cu // NMC and d.). Charge-Discharge profile Au-3D-Cu // NMC

4.1.2 Charge-Discharge with 2M LiTFSI Liquid Electrolyte

Furthermore, with poor cyclability from the previous cycling with LiPF6 electrolyte resulting to capacity decay, a high concentration of electrolyte 2M LiTFSI electrolyte in FEC / DMC / EC (1:1:1 v/v) was used to assemble new battery and cycled them for another charge-discharge process, to compare the charge-discharge capacity, Au-2D-Cu || NCM was cycled with 0.2 C and initial charge capacity of around 200 mAh g^{-1} and discharge capacity of 110 mAh g^{-1} with a CE of 80% after 3 cycles, the reversibility of the lithium ion was more steady because of

the presence of more lithium present in the electrolyte salts compensated the limited lithium in the cathode electrode which helped to maintain more lithium-ion reversibility in **fig. 18b**.

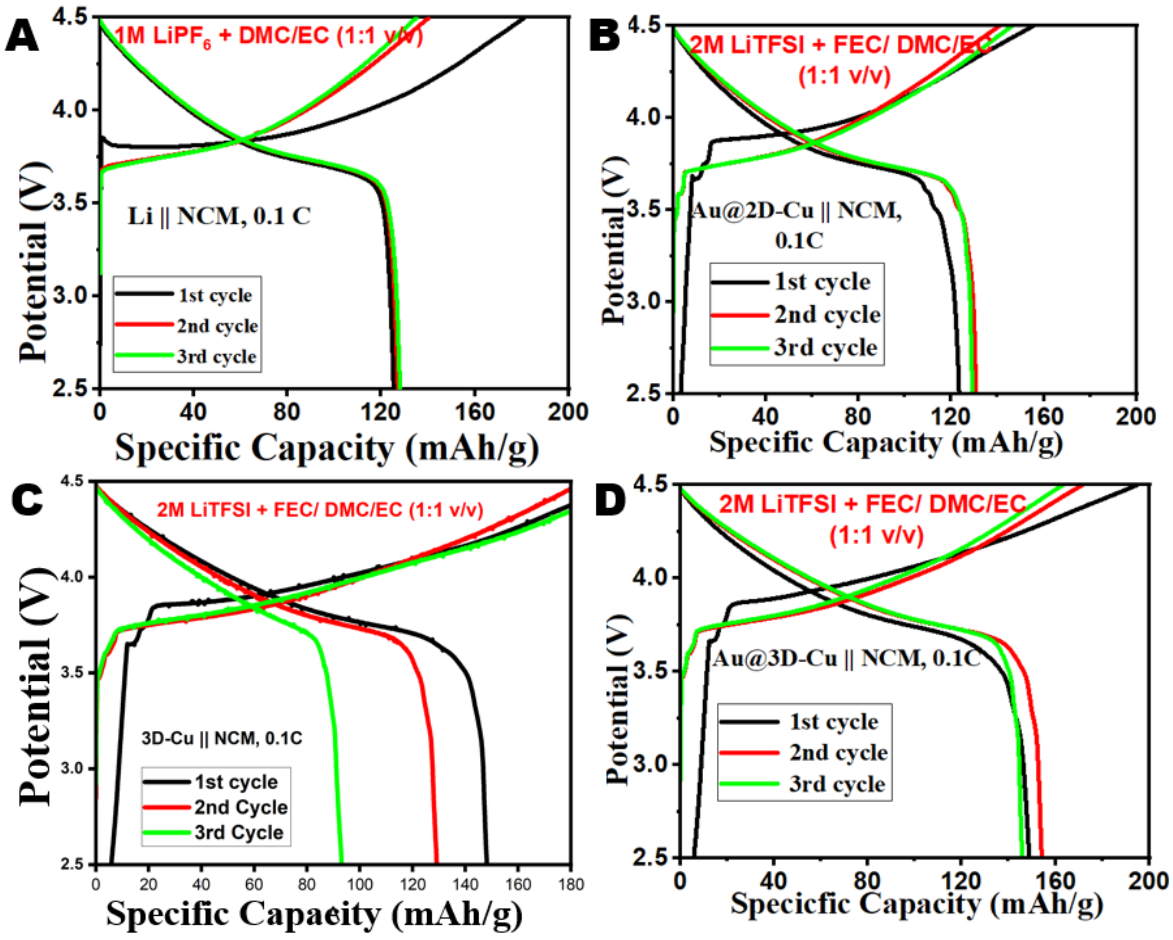

Figure 18*; first charge-Discharge profile with 2M $LiTFSI_6$ liquid electrolyte a). Charge-Discharge profile of Li // NCM, b.) Charge-Discharge profile 3Cu // NMC c.) Charge-Discharge profile Au@2D-Cu // NMC and d.). Charge-Discharge profile Au@3D-Cu // NMC*

3D-Cu || NCM was also cycled, at 0.2 C, the initial reversible capacity was above 180 mAh g^{-1} and 150 mAh g^{-1} with CE 84 %, however after 3 cycles, the capacity decay drastically reduced as the cycling continued, the non-modified copper foam current collector affected the capacity decay in **Fig. 18c.** While in **Fig. 18d,** the initial charge-discharge rate was maintained above 180 mAh g-1

and 155 mAh g-1, respectively, and more reversible lithium-ion was seen after 3 cycles with 90% CE. The modification of the Au-3D-Cu || NCM contributed to the more steady reversibility capacity, but capacity decay occurred after 10 cycles, which became a concern for further improvement.

4.1.3 Tri-Lithium salt electrolyte optimization

In the selection of lithium-ion salts that could solve the problems of anodeless lithium-ion battery is a critical part of the electrolyte optimization. Firstly, the electrolyte solvent was carefully selected which includes; fluoroethylene carbonate (FEC) and dimethyl ethylene (DME). The selection of these solvent is based on the effect of the both solvent delivering passivation on the deposited lithium at the anode electrode, capacity loss reduction, maintained good reversibility of lithium-ion over a long period of time, and visco-electrolyte effect to the cell for a lasting electrochemical performance.

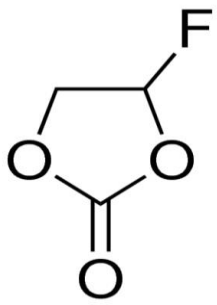

Fluoroethylene carbonate (FEC)

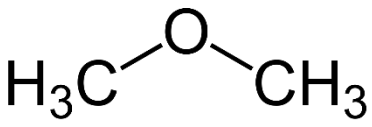

Dimethyl ethylene (DME)

On the other hand, three suitable lithium salts has been carefully selected with the proportion of 1.5M lithium bis(trifluoromethanessulfonyl), 1M lithium difluoro(oxalate) borate (LIDFOB), and 0.05M lithium hexafluorophosphate (LIPF6) as an additive. The combination of this lithium salts delivers high CE, corrosion inhibitors to the current collector and and compensate the limited lithium-ion in the cell.

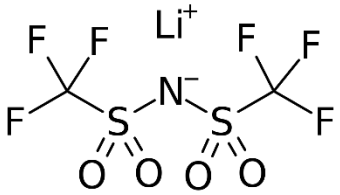

1.5M lithium bis (Trifluoromethanessulfonyl)

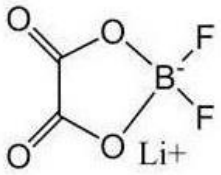

1M lithium difluoro(oxalate) borate (LIDFOB)

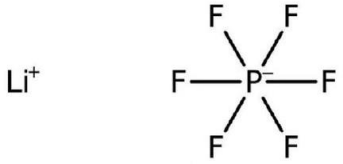

0.05M lithium hexafluorophosphate (LIPF6)

4.1.3 Charge-Discharge profile with Dual salt liquid electrolytes

Lastly, more investigation was done by using a tri-salt electrolyte to achieve high capacity similar to the theoretical capacity of traditional NCM-Lithium-metal battery. In this case, 1.5M LiTFSI + 1M LiDFOB of lithium salt with 0.05M LiPF6 as an additive was used in FEC/DME (2:3 v/v). In **Fig. 19a,** 2D-Cu || NCM charge-discharge profile delivers charge capacity of above 180 mAh g-1 and a discharge capacity of 166 mAh g^{-1} with a CE of 90% at 0.2 C. After 8 cycles, the reversibility of lithium-ion reduced to 130 mAh g^{-1}. This capacity reduction attributed to the non-coated effect of 2D-Cu current collector. In **Fig. 19b**, Au-2D-Cu || NCM showed a very good cyclability with a capacity of 161 mAh g^{-1} and later dropped to 159 mAh g^{-1} with a CE of 99.9% at 0.2 C after 8 cycles because the coated gold on the surface of the current collector helped to provide more nucleation sited for lithium deposition. Also, the results from **Fig. 19c** shows a high capacity loss with charge-discharge capacities of 161 mAh g^{-1} in the first cycle and 110 mAh g^{-1} capacity after 8 cycles, maintaining 98% CE at 0.2 C. This is because of non-coated effect of the 3D-Cu current collector. In **Fig.19d**. The first charge-discharge capacity showed above 180 mAh g^{-1} and 182 mAh g^{-1} with a CE of 99.99% at 0.2 C after 8 cycles, the high reversibility capacity dropped to 160 mAh g^{-1}. The two modified copper current collectors show similar electrochemical performance, with Au-3D-Cu || NCM having high charge-discharge capacities even after 50 cycles which is demonstrated with cyclic performance in Fig. 20. The LiDFOB salt in the electrolyte ensured excellent stripping and plating, and enhanced the passivation of Al foil current collector against corrosion. Also, the addition of the LiPF6 as an additive assisted specifically for high

capacity of the battery, while LiTFSI salt ensured the formation of a stable SEI, preventing cracking of the Li deposit at the anode electrode. In conclusion, the dual salt electrolyte with ether-based solvent used ensured excellent interfacial contact between the electrolyte and the current collector and good stability of the lithium deposit.

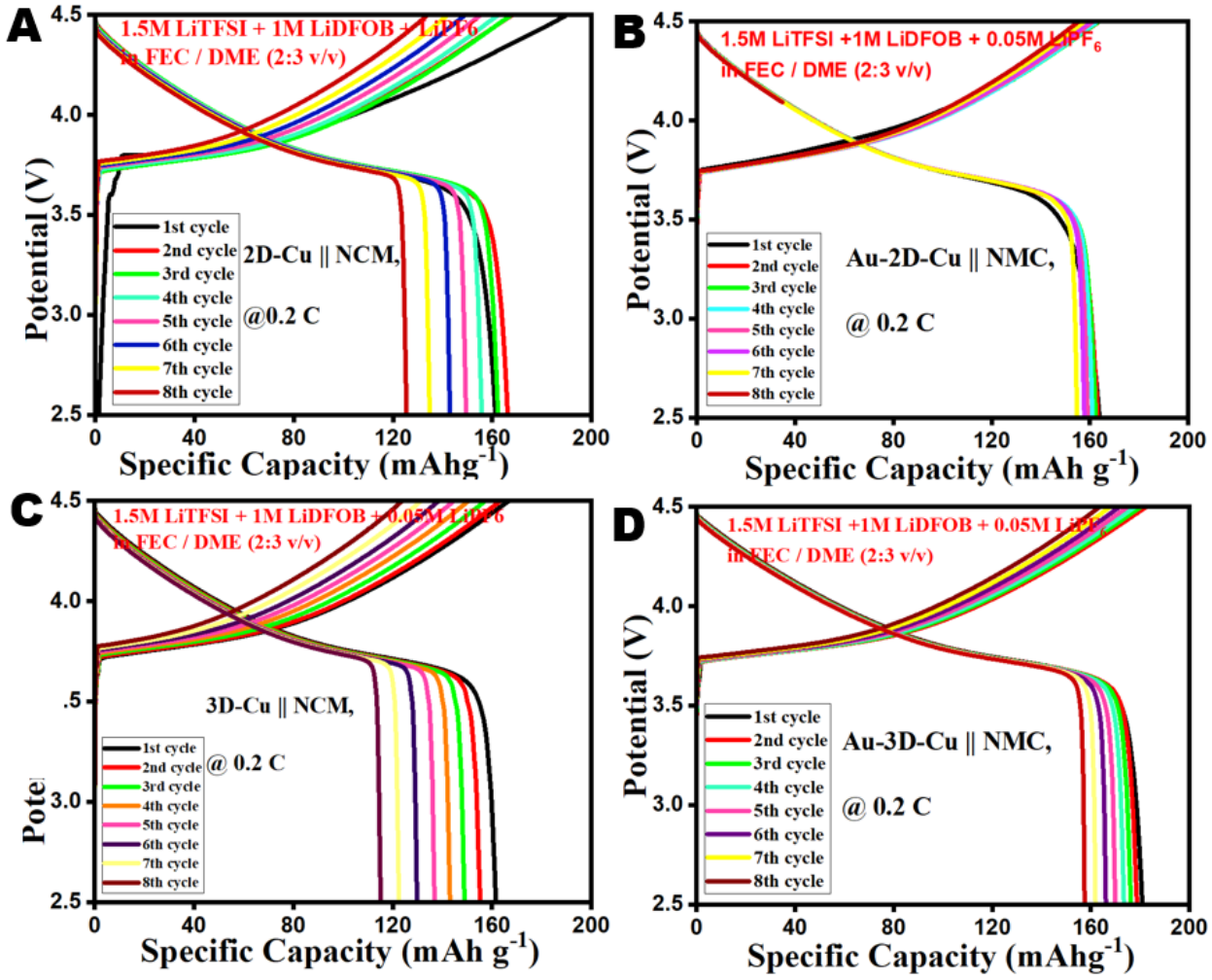

Figure 19; Charge-Discharge profile with 1.5M LiTFSI + 1M LiDFOB + 0.05M $LiPF_6$ liquid electrolyte a). Charge-Discharge profile of 2D-Cu // NCM, b.) Charge-Discharge profile of 3Cu // NMC c.) Charge-Discharge profile of Au@2D-Cu // NMC and d.). Charge-Discharge profile of Au@3D-Cu // NMC

4.1.4 Cyclic Performance of the cell

To further explore the cyclic performance of the batteries after several cycles, the 2D-Cu || NCM, 3D-Cu || NCM, Au-2D-Cu || NCM, and Au-3D-Cu || NCM full cells were assembled with 1.5M LiTFSI + 1M LiDFOB, + 0.05M LiPF6 in FEC/DDME (2:3 v/v) at 0.2 C, and the cycling potentials were 2.5 V–4.5 V. The batteries in **Fig. 20** were galvanostatically placed on 50 cycles. The initial discharge capacities of 2D-Cu || NCM, 3D-Cu || NCM, and Au-2D-Cu || NCM were approximately 160 mAh g^{-1} except for Au-3D-Cu || NCM, which recorded approximately 185 mAh g^{-1} at first discharge capacity before starting to decrease. After 50 cycles, the reversible capacity, in **Fig. 20a** (2D-Cu || NCM) dropped to 20 mAh g^{-1} with a CE of 97%, in **Fig. 20b,** the first discharge capacity of 161 mAh g^{-1} of 3D-Cu || NCM with a CE of 89% was observed, and after 50 cycles, the reversible capacity reduced to 80 mAh g^{-1}.

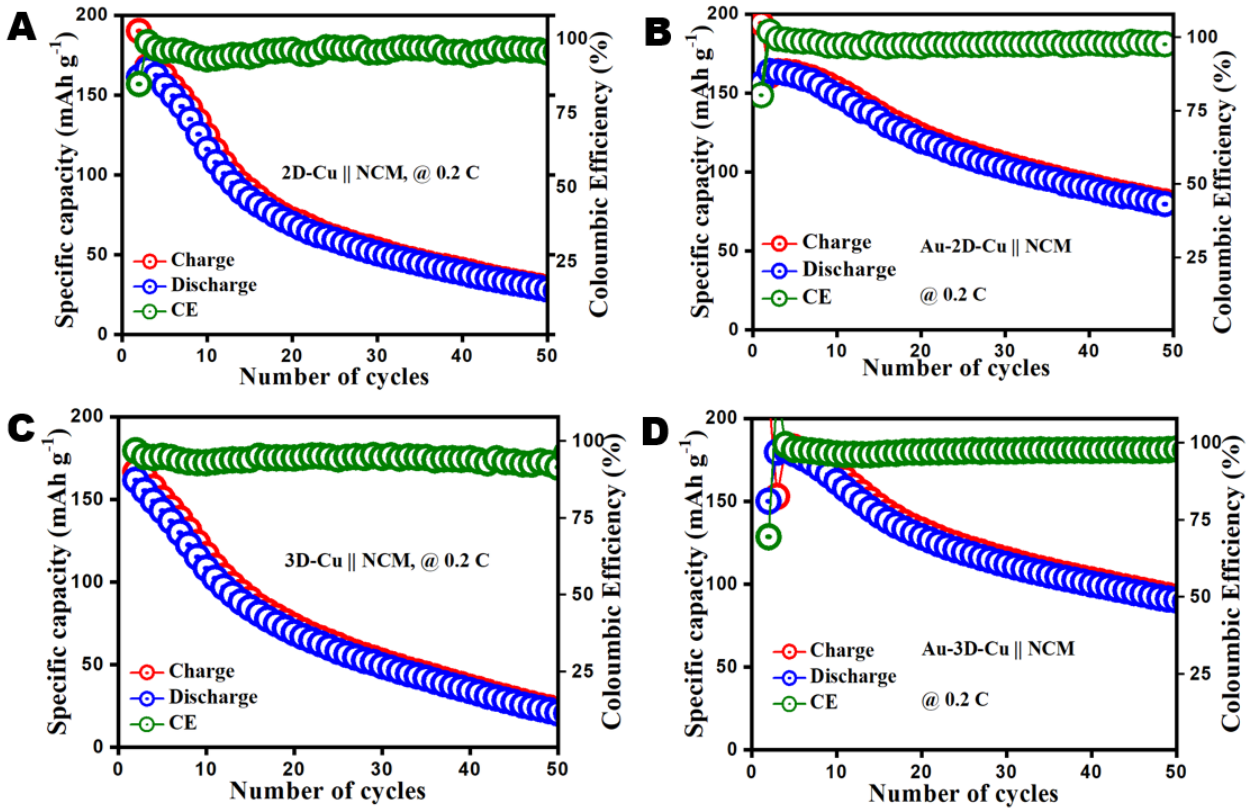

Figure 20; Cyclic Performance process of all the copper current collector.

On the other hand, 3D-Cu || NCM shows the first discharge capacity In **Fig. 20c** with 170 mAh g-[1], with CE of 97% and after 50 cycle the capacity drastically reduced to 15 mAh g-[1]. Then finally, in **Fig 20d**, showed the first discharge capacity of 180 mAh g-[1] an overall discharge capacity of 95 mAh g^{-1} after 50 cycles with a steady CE efficiency of 99.99%. Therefore in conclusion, **Fig 20d** shows an excellent cyclic performance when compared with other current collectors, so this results of Au-3D-Cu || NCM still confirmed the sputtering effect of the gold material on the surface of the current collector and advantageous effect of the new optimized tri-lithium salt electrolyte which provided stability for lithium deposits. Therefore, the reversibility of lithium during stripping and plating was successfully uniform.

4.1.5 Rate capability

In another experiment to evaluate the effect of the battery at different C-rate, the coated Au-2D-Cu || NCM and Au-3D-Cu || NCM, was investigated. The full-cells were assembled with a liquid electrolyte of 1.5M LiTFSI + 1M LiDFOB, + 0.05M LiPF6 in FEC/DDME (2:3 v/v), cycling potential ranges of 2.5V and 4.5V, and capacity discharge rates of 0.2C to 2C. The results revealed that the Au-2D-Cu || NCM full-cell could provide a capacity of about 161 mAh g^{-1} at a discharge rate of 0.2 C, however, the discharge capacity reduced as the rate capacity increased from 0.2 C to 2 C. The capacity could recover to around 80 mAh g^{-1} when the rate returned to 0.2 C. In comparison to Au-3D-Cu || NCM which showed a first reversible capacity of 181 mAh g^{-1} at a rate capacity of 0.2 C and decreased steadily as the rate capacity increased from 0.2 C to 2 C. However, it had better C-rate performance than the Au-2D-Cu || NCM and could deliver a high capacity with a recovering capacity of approximately 100 mAh g^{-1} when the rate returned to 0.2 C. This makes Au-3D-Cu || NCM a promising option with excellent rate capability for practical applications.

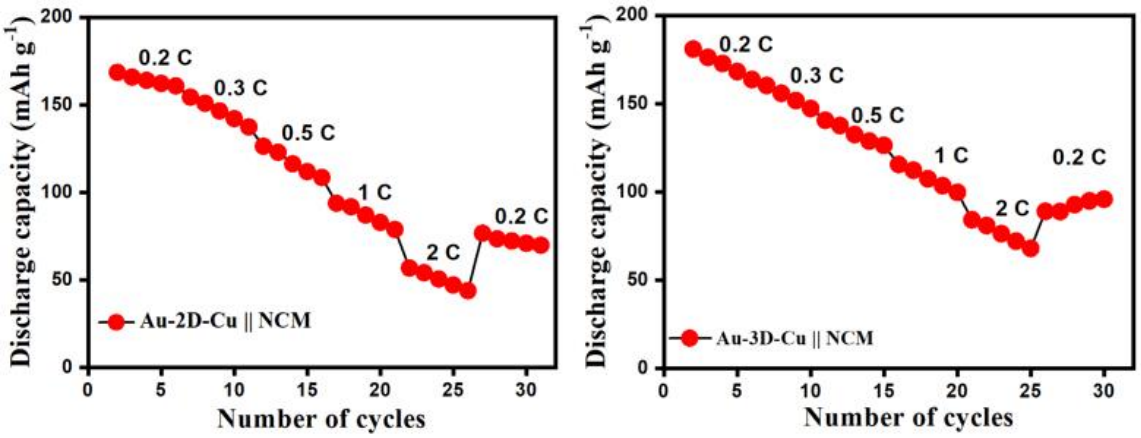

Figure 21; Rate Capability

Therefore, in summary from the experimental results, the charge-discharge profile, cyclic performance and rate capability has proven that Au-3D-Cu || NCM shows an excellent electrochemical performance which made it the best candidate for anodeless rechargeable lithium-ion battery. This great performance was possible because of the sputtering effect of gold on the surface of the 3D-Cu || NCM and the application of the tri-lithium salt liquid electrolyte

4.2 Post mortem analysis

Post mortem analysis was carried out to observe the changes in the morphology and structure on the surface of the current collectors. Au-2D-Cu || NCM, and Au-3D-Cu || NCM after 100 cycles as seen in **Fig. 22**

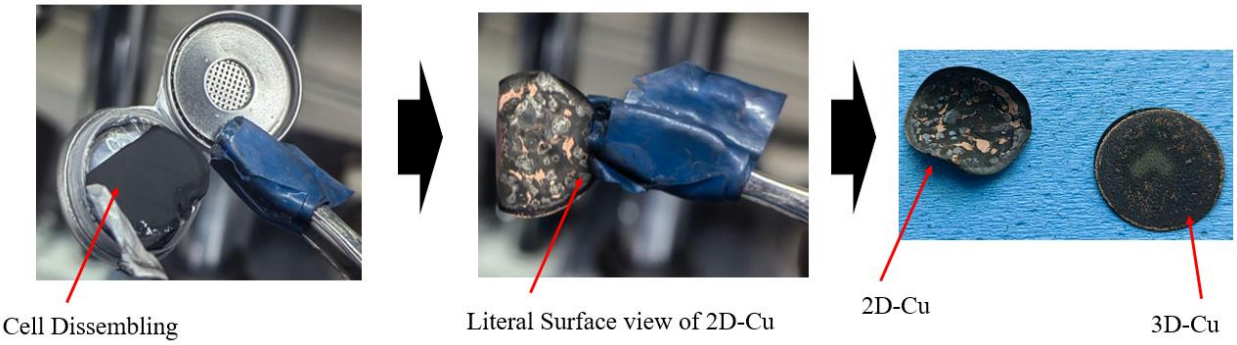

Figure 22: ***dissembling process of Au-2D-Cu || NCM and Au-3D-Cu || NCM for post mortem analysis.***

After disassembling the cell in the glove box, the copper current collectors were washed with DME solvent to remove the traces of electrolyte and ketp in the glove box for 24 hours and later dried in an oven for 1 hour at 60^0C. The copper current collectors were investigated using SEM to compare the surface morphology of the current collectors and dendrite formation after 100 cycling. **Fig.23 a and d.** showed the rough surface of lithium deposits on Au-2D-Cu || NCM and Au-3D-Cu || NCM with LiTFSI electrolyte as shown in **Fig. 18**. **Fig.23 b and e** showed a very smooth lithium deposits on the surfaces of the modified Au-2D-Cu || NCM and Au-2D-Cu || NCM. The smoothness of the lithium deposits on the surface of the modified current collectors resulted from the choice of 1.5M LiTFSI + 1M LiDFOB, + 0.05M LiPF6 in the FEC/DDME (2:3 v/v) tri-lithium salt electrolytes used. The application of this electrolyte also offered a stable SEI which protected the deposited lithium metal on the surface of the current collectors from cracking and made the anode-less LIBs dendrites free. **Fig. 23c** illustrates the cross section of the deposited lithium on the surface of the Au-2D-Cu ||NCM after cycling, which is about 25.31 µm confirming the uneven deposition of the lithium on the surface of the Au-2D-Cu || NCM, while **Fig. 24f** also shows a smooth cross sectional area of the deposited lithium on the surface of the Au-3D-Cu || NCM copper after cycling with a thickness of 44.71 µm as can be seen below.

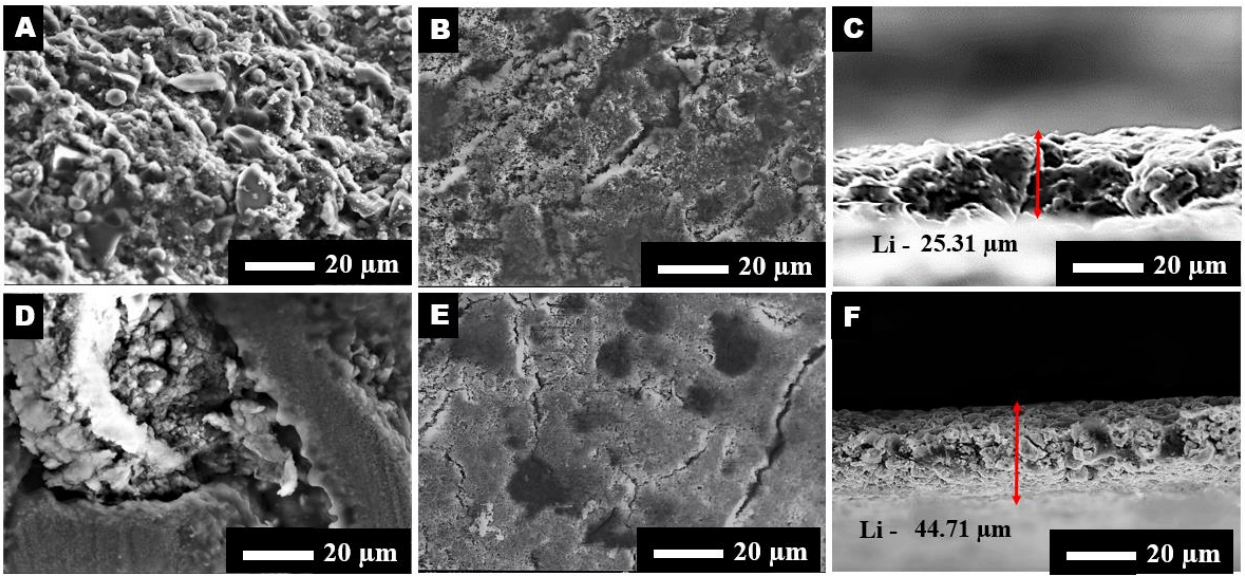

Figure 23*: SEM image of Au-2D-Cu || NCM and Au-3D-Cu || NCM after dissembling process.*

5.0 Chapter 5 – Conclusion

In summary, an Au-coated 3-D-Cu current collector was developed and investigated as an anode material for anode-less rechargeable LIBs. The porous 3D-Cu structure successfully provided multiple lithium nucleation sites, and enabled lithium intercalation into the micro - channels of the 3D structure, making it a superior option than a 2D planar structure. While the lithiophilic gold layers sputtered on the surface of the copper current collector also aided in stabilizing lithium deposition and reduced the local current density. This synergy allowed lithium to be uniformly deposited into the internal scaffolding of the Au-3D-Cu current collector as an effective strategy for suppressing dendrite growth. The optimization of a suitable liquid electrolyte in the ratio of 1.5M LiTFSI + 1M LiDFOB with 0.05M $LiPF_6$ as an additive in FEC / DME (2:3 v/v) solvents greatly improved the electrochemical performance of the Au-3D-Cu||NCM, forming a stable SEI which protected the deposited lithium at the anode from cracking. Importantly, the full-cell Au-3D-Cu||NCM after 50 cycles achieved a reversible capacity of up to 120 mAh g^{-1} with a CE of 99.9%, which is a very remarkable result when compared to the capacity results from Au-2D-Cu||NCM. Therefore, the selection of copper current collector as anode material, fabrication of anodeless, achieving excellent electrochemical performance and solving the problem of dendrite growth generally confirmed that the aim and objectives of this research was successfully met which offered this study a fresh opportunity to produce high-performance dendrite-free anode-less batteries by designing a lithiophilic 3D structural current collector as the next generation material for LIBs.

Reference List

1. **Zhao, W.,** A forum on batteries: from lithium-ion to the next generation. Natl Sci Rev, 2020. **7**(7): p. 1263-1268.
2. **Liu, B., J.-G. Zhang, and W. Xu,** Advancing Lithium Metal Batteries. Joule, 2018. **2**(5): p. 833-845.
3. **Brotchie,** A., Borophene: Served on a silver platter. Nature Reviews Materials, 2016. **1**(11): p. 16083.
4. **Xie, Z., et al.,** A ternary FeS2/Fe7S8@nitrogen-sulfur co-doping reduced graphene oxide hybrid towards superior-performance lithium storage. Progress in Natural Science: Materials International, 2021. **31**(2): p. 207-214.
5. **Shi, L., et al.**, Early Failure of Lithium-Sulfur Batteries at Practical Conditions: Crosstalk between Sulfur Cathode and Lithium Anode. 2022. **9**(21): p. e2201640.
6. **Lin, D., Y. Liu, and Y. Cui,** Reviving the lithium metal anode for high-energy batteries. Nat Nanotechnol, 2017. **12**(3): p. 194-206.
7. **Yim, C.-H., et al.,** Understanding key limiting factors for the development of all-solid-state-batteries. Chemical Engineering Journal Advances, 2023. **13**: p. 100436.
8. **Heim, F., T. Kreher, and K.P. Birke** The Influence of Micro-Structured Anode Current Collectors in Combination with Highly Concentrated Electrolyte on the Coulombic Efficiency of In-Situ Deposited Li-Metal Electrodes with Different Counter Electrodes. Batteries, 2020. **6**, DOI: 10.3390/batteries6010020.
9. **Cheng, X.B., et al.,** A Review of Solid Electrolyte Interphases on Lithium Metal Anode. Adv Sci (Weinh), 2016. **3**(3): p. 1500213.
10. **Liu, Y., X. Meng, and Z. Wang,** A Li(2)S-based all-solid-state battery with high energy and superior safety. 2022. **8**(1): p. eabl8390.
11. **Liu, M., et al.,** Controlling the Lithium-Metal Growth To Enable Low-Lithium-Metal-Excess All-Solid-State Lithium-Metal Batteries. ACS Materials Letters, 2020. **2**(7): p. 665-670.
12. **Wang, M.J., et al.,** Enabling “lithium-free” manufacturing of pure lithium metal solid-state batteries through in situ plating. Nature Communications, 2020. **11**(1): p. 5201.

13. **Krauskopf, T., et al.**, Physicochemical concepts of the lithium metal anode in solid-state batteries. Chemical reviews, 2020. **120**(15): p. 7745-7794.
14. **Ryou, M.H., et al.,** Mechanical surface modification of lithium metal: towards improved Li metal anode performance by directed Li plating. Advanced Functional Materials, 2015. **25**(6): p. 834-841.
15. **Jana, A., et al.**, Electrochemomechanics of lithium dendrite growth. Energy & Environmental Science, 2019. **12**(12): p. 3595-3607.
16. **Zhao, J., et al.**, Surface fluorination of reactive battery anode materials for enhanced stability. Journal of the American Chemical Society, 2017. **139**(33): p. 11550-11558.
17. **Wang, G., et al.,** Self-stabilized and strongly adhesive supramolecular polymer protective layer enables ultrahigh-rate and large-capacity lithium-metal anode. Angewandte Chemie International Edition, 2020. **59**(5): p. 2055-2060.
18. **Betz, J., et al.,** Theoretical versus practical energy: a plea for more transparency in the energy calculation of different rechargeable battery systems. Advanced energy materials, 2019. **9**(6): p. 1803170.
19. **Niu, C., et al.,** High-energy lithium metal pouch cells with limited anode swelling and long stable cycles. Nature Energy, 2019. **4**(7): p. 551-559.
20. **Xiang, J., et al.**, Alkali-metal anodes: from lab to market. Joule, 2019. **3**(10): p. 2334-2363.
21. **Yang, H., et al.,** Recent progress and perspective on lithium metal anode protection. Energy Storage Materials, 2018. **14**: p. 199-221.
22. **Qian, J., et al.,** Anode-free rechargeable lithium metal batteries. Advanced Functional Materials, 2016. **26**(39): p. 7094-7102.
23. **Mashtalir, O., et al.**, High-purity lithium metal films from aqueous mineral solutions. ACS omega, 2018. **3**(1): p. 181-187.
24. **Aurbach, D.,** Review of selected electrode–solution interactions which determine the performance of Li and Li ion batteries. Journal of Power Sources, 2000. **89**(2): p. 206-218.
25. **Weng, W., V.G. Pol, and K. Amine,** Ultrasound assisted design of sulfur/carbon cathodes with partially fluorinated ether electrolytes for highly efficient Li/S batteries. Advanced materials, 2013. **25**(11): p. 1608-1615.

26. **Cao, X., et al.**, Nonflammable electrolytes for lithium ion batteries enabled by ultraconformal passivation interphases. ACS Energy Letters, 2019. **4**(10): p. 2529-2534.
27. **Sodeyama, K., et al.,** Sacrificial anion reduction mechanism for electrochemical stability improvement in highly concentrated Li-salt electrolyte. The Journal of Physical Chemistry C, 2014. **118**(26): p. 14091-14097.
28. **Fan, X., et al.**, Highly fluorinated interphases enable high-voltage Li-metal batteries. Chem, 2018. **4**(1): p. 174-185.
29. **Ren, X., et al.**, High-concentration ether electrolytes for stable high-voltage lithium metal batteries. ACS Energy letters, 2019. **4**(4): p. 896-902.
30. **Zhang, X., Y. Yang, and Z. Zhou,** Towards practical lithium-metal anodes. Chemical Society Reviews, 2020. **49**(10): p. 3040-3071.
31. **Hagos, T.T., et al.,** Locally concentrated LiPF6 in a carbonate-based electrolyte with fluoroethylene carbonate as a diluent for anode-free lithium metal batteries. ACS applied materials & interfaces, 2019. **11**(10): p. 9955-9963.
32. **Borodin, O., et al.,** Uncharted waters: super-concentrated electrolytes. Joule, 2020. **4**(1): p. 69-100.
33. **Wang, Z., et al.,** Nano-Cu-embedded carbon for dendrite-free lithium metal anodes. Journal of Materials Chemistry A, 2019. **7**(40): p. 22930-22938.
34. **Chen, J., et al.,** Dynamic intelligent Cu current collectors for ultrastable lithium metal anodes. Nano Letters, 2020. **20**(5): p. 3403-3410.
35. **Gu, Y., et al.,** Lithiophilic faceted Cu (100) surfaces: high utilization of host surface and cavities for lithium metal anodes. Angewandte Chemie International Edition, 2019. **58**(10): p. 3092-3096.
36. **Ding, F., et al.**, Dendrite-free lithium deposition via self-healing electrostatic shield mechanism. Journal of the American Chemical Society, 2013. **135**(11): p. 4450-4456.
37. **Ding, F., et al.**, Effects of cesium cations in lithium deposition via self-healing electrostatic shield mechanism. The Journal of Physical Chemistry C, 2014. **118**(8): p. 4043-4049.
38. **Duan, H., et al.**, Uniform nucleation of lithium in 3D current collectors via bromide intermediates for stable cycling lithium metal batteries. Journal of the American Chemical Society, 2018. **140**(51): p. 18051-18057.

39. **Hu, A., et al.**, An artificial hybrid interphase for an ultrahigh-rate and practical lithium metal anode. Energy & Environmental Science, 2021. **14**(7): p. 4115-4124.
40. **Cheng, X.-B., et al.,** Nanodiamonds suppress the growth of lithium dendrites. Nature communications, 2017. **8**(1): p. 336.
41. **Chen, W., et al.,** Lithiophilic montmorillonite serves as lithium ion reservoir to facilitate uniform lithium deposition. Nature Communications, 2019. **10**(1): p. 4973.
42. **Yan, K., et al.,** Selective deposition and stable encapsulation of lithium through heterogeneous seeded growth. Nature Energy, 2016. **1**(3): p. 1-8.
43. **Li, G., et al.**, Self-assembly of porous CuO nanospheres decorated on reduced graphene oxide with enhanced lithium storage performance. RSC advances, 2017. **7**(17): p. 10376-10384.
44. **Yu, J., et al.,** Graphene-modified 3D copper foam current collector for dendrite-free lithium deposition. Frontiers in chemistry, 2019. **7**: p. 748.